CRYSTALLOGRAPHIC INVESTIGATIONS OF

$C_{27}H_{34}N_2O_4ClRh$

136814

A Thesis Submitted to the

Graduate School of Natural and Applied Sciences of

Dokuz Eylül University

In Partial Fulfillment of the Requirements for

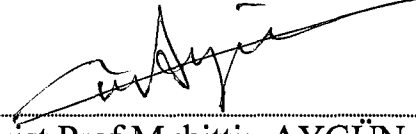The Degree of Master of Science in Physics

by

Aslıhan KARTAL

September, 2003

İZMİR

Ms.Sc. THESIS EXAMINATION RESULT FORM

We certify that we have read the thesis, entitled **"CRYSTALLOGRAPHIC INVESTIGATIONS OF $C_{27}H_{34}N_2O_4ClRh$"** completed by **ASLIHAN KARTAL** under supervision of **ASSIST.PROF.MUHİTTİN AYGÜN** and that in our opinion it is fully adequate, in scope and in quality, as a thesis for the degree of Master of Science.

Assist.Prof.Muhittin AYGÜN

Supervisor

Prof.Dr.Kemal KOCABAŞ

Committee Member

Prof.Dr.Mustafa EROL

Committee Member

Approved by the

Graduate School of Natural and Applied Sciences

Prof.Dr.Cahit Helvacı

Director

ACKNOWLEDGEMENTS

ABSTRACT

Molecular and crystal structure of, "1,3-Bis(2,4-dimethoxyphenyl)imidazolidin-2-ylidenechloro(1,5-cyclooctadiene)rhodium(I)", ($C_{27}H_{34}N_2O_4ClRh$), has been determined by single crystal X-ray diffraction method. Crystallographic data for $C_{27}H_{34}N_2O_4ClRh$: Triclinic, P-1, $a = 9.7642(12)$Å, $b = 11.1914(11)$Å, $c = 13.0102(14)$Å, $Z = 2$, $D_x = 1.531(g/cm^3)$, $\mu(MoK_\alpha) = 0.809mm^{-1}$, V=1277.59(71) Å^3, $F_{000} = 607.9$, $R_1 = 0.041$, $wR_2 = 0.091$, GOF=1.025, $\Delta\rho_{min} = -0.537$ e/Å^3, $\Delta\rho_{max} = 0.576$ e/Å^3, $(\Delta/\sigma)_{max} = 0.087$. The crystal structure was solved by Patterson method. Using full matrix least-square and difference-Fourier methods, the 316 atomic parameters were refined to a final R= 0.041 for 2983 reflections with $I > 2\sigma(I)$. The non-hydrogen atoms were refined anisotropically. The four atoms, Rh1, Cl1, C20 and C21 form a plane; also the carbene ligand is nearly planar. The angle between the carbene heterocycle and the coordination plane is 89.8(4)°. Because of the trans influences of the chelating ligand the bond distances of the Rh-C20 and Rh-C21 are shorter than the Rh-C24 and Rh-C25. Metal-C(carbene) bond length is virtually the same as Metal-C(hydrocarbyl) bonds. The C(carbene)-N bond lengths is significantly shorter than the other C-N bond lengths present in the complex and is possibly indicative of greater partial double bond character in these C(carbene)-N bonds due to partial electron donation by nitrogen to the carbene carbon. Cl-Rh-$C_{carbene}$ angle 90.0(1)°. The imidazole heterocycle makes dihedral angles of 76.8(3)° and 77.3(3)° with the methoxyphenyl ring planes, respectively. In addition the dihedral angle between two methoxyphenyl ring planes is 29.3(2)°. And the crystal structure is stabilized by two weak intermolecular hydrogen bond of the C-H....Cl type.

ÖZET

"1,3-Bis(2,4-dimetoksifenil)imidazolidin-2-ylidenekloro(1,5-siklooktadien) rodyum (I)", ($C_{27}H_{34}N_2O_4ClRh$), molekülünün moleküler ve kristal yapısı tek kristal x-ışını kırınımı yöntemiyle çözülmüştür. $C_{27}H_{34}N_2O_4ClRh$ molekülü için kristalografik veriler: Triklinik, P-1, $a = 9.7642(12)$Å, $b = 11.1914(11)$Å, $c = 13.0102(14)$Å, $Z = 2$, $D_x = 1.531$(g/cm^3), μ(MoK$_\alpha$)=0.809mm^{-1}, V=1277.59(71) Å^3, F_{000}= 607.9, R$_1$=0.041, wR$_2$ = 0.091, GOF=1.025, $\Delta\rho_{min}$ = -0.537 e/Å^3, $\Delta\rho_{max}$ = 0.576 e/Å^3, $(\Delta/\sigma)_{max}$ = 0.087. Kristal yapı Patterson yöntemi ile çözülmüştür. 316 atomik parametre, $I > 2\sigma(I)$ koşulunu sağlayan 2983 yansıma için tam matris en küçük kareler ve fark- Fourier yöntemleri kullanılarak R=0.041 değerine kadar arıtılmıştır. Hidrojen atomları hariç tüm atomlar anizotropik olarak arıtılmıştır. Rh1, Cl1, C20, C21 atomlarının bir düzlem oluşturduğu saptanmıştır. Karben ligandı da hemen hemen düzlemseldir. Karben heterosiklik ile koordinasyon düzlemi arasındaki açının 89.8(4)° olduğu tespit edilmiştir. Şelat yapıcı ligandın trans etkilerinden dolayı Rh-C20 ve Rh-C21 atomları arasındaki bağ uzunlukları, Rh-C24 ve Rh-C25 arasındaki bağ uzunluklarından kısadır. Yapıdaki Metal-C(karben) bağ uzunluğu, Metal-C(hidrokarbil) bağ uzunlukları ile hemen hemen aynıdır. Karben karbonu ile azot arasındaki bağ uzunlukları kompleksdeki öteki C-N bağ uzunluklarından kısadır. Çünkü donor N atomlarından karben karbonuna kısmi elektron akışı, bu bağların nispeten çift bağ karakteri göstermesini sağlar. Cl-Rh-$C_{carbene}$ atomları arasındaki açı 90.0(1)°. İmidazol heterosikliğin, metoksifenil halka düzlemleri ile yaptığı dihedral açı sırasıyla 76.8(3)° ve 77.3(3)°. Ayrıca iki metoksifenil halka arasındaki dihedral açı 29.3(2)°. Ve kristal yapı moleküller arası C-H ...Cl tipi zayıf iki hidrojen bağı ile kararlı durumdadır.

CONTENTS

Chapter One

INTRODUCTION

Chapter Two

X-RAYS AND X-RAY DIFFRACTION DATA

Chapter Three
SOLUTION OF CRYSTAL STRUCTURES

Chapter Four
CRYSTAL REFINEMENT

Chapter Five
EXPERIMENTAL DETAILS

Chapter Six
CONCLUSION

LIST OF TABLES

LIST OF FIGURES

CHAPTER ONE

INTRODUCTION

1.1 Introduction

In this research, the crystal structure of "1,3-Bis(2,4-dimethoxyphenyl)imidazolidin-2-ylidenechloro(1,5-cyclooctadiene)rhodium(I)", ($C_{27}H_{34}N_2O_4ClRh$), which is functionalized N-heterocyclic carbenes (NHCs) complex, is determined by single crystal X-ray diffraction technique. The chemical diagram of the title compound is given in Figure 1.1.
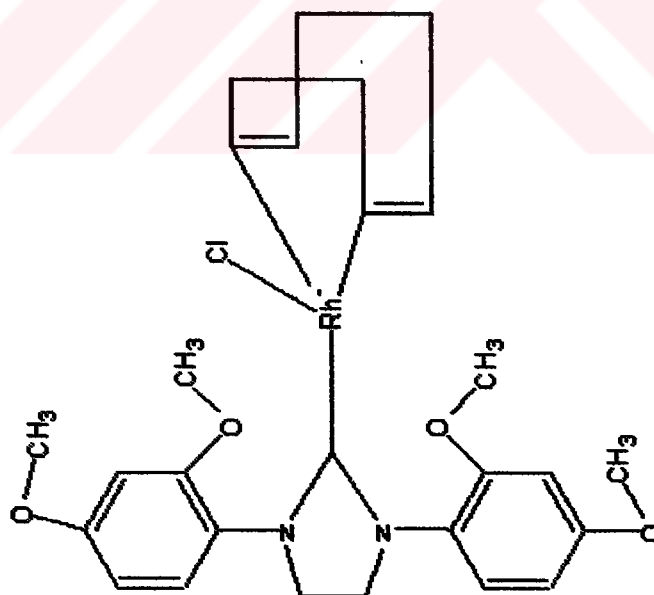
Figure 1.1 The chemical diagram of the title compound.

NHCs based on the imidazol(in)ium ring system, 1 and 2, respectively, have proven to be versatile and important class of ligands both in organometallic chemistry and homogeneous catalysis; they tend to coordinate very strongly to the metal centers (Weskamp et al., 2000; Bourissou et al., 2000; Herrmann, 2002; Lappert, 1988).
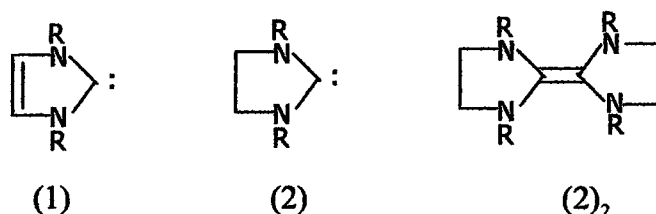
Figure 1.2 (1):imidazolin-2-ylidene, (2):imidazolidin-2-ylidene,

$(2)_2$:Dimerized form of (2)

The dimerized form $(2)_2$ of the (2) have reactivity characteristic of nucleophilic carbenes (Lappert, 1988). Some typical procedures employed to prepare complexes of saturated NHC's with linear or cyclic groups are presented in Eqn. 1, 2. Deprotonation of imidazolinium salts (3, Eqn. 1) and cleavage of C=C bond of the alkene (4, Eqn. 2) [Weskamp et al., 2000; Bourissou et al., 2000; Herrmann, 2002] occupy a prominent place.
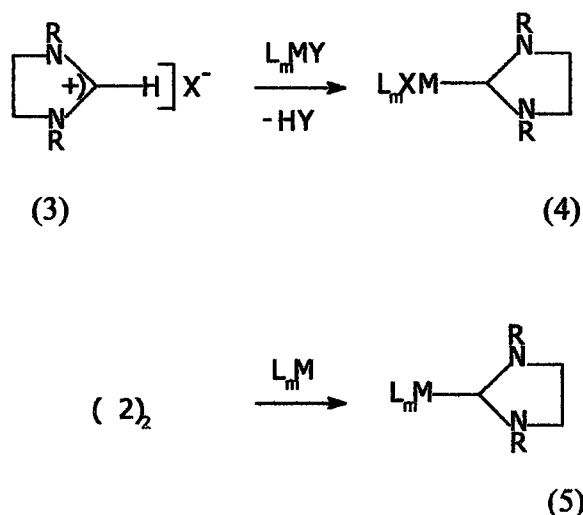
Figure 1.3 The general synthesis method of saturated carbene-metal complexes.

N-heterocyclic carbene (NHCs) complexes of late transition metals have been the focus of increasing interest due to the unique electronic properties of the carbene ligands (Herrmann, 2002; Herrmann & Köcher, 1997; Huang et al., 1999; Arduengo et al., 1992). The donation of electron density by the nitrogen substituents on the carbene makes the carbene carbon nucleophilic and compensates for the electron flow from the carbon to the metal. Donation from the nitrogens is such that the carbene carbon may actually become a partial π-donor (Herrmann (b) et al., 1995; Fröhlich et al., 1997). Heterocyclic carbenes are thus pure donor ligands. They have similarities to the tertiary phosphines but appear to be stronger coordinating ligands which undergo little or no dissociation from the metal in solution (Lappert, 1975).

After the Herrmann, who first showed NHCs being used as ligands in active catalysts, numerous literatures, some of which are (Herrmann (b) et al., 1997; Green et al., 1998; Çetinkaya et al., 1997; McGuinness et al., 1998; Herrmann et al., 1998; Danopoulos et al., 2002; Weskamp et al., 1999; Vazquez-Serrano et al., 2002), have been published on the NHCs metal complexes employed as homogeneous catalysis.

Generally, in these reports, wide variety functional groups on the N-atoms of NHCs ligands have been added to improve catalytic properties of the complexes with many transition elements.

NHCs have shown promise as replacements for the commonly used, air sensitive phosphine-based class of ligands.

NHCs and phophine ligands have also been combined in some metal complexes. This combination results in improvement of the catalytic properties and stability of the compounds under the reaction condition (McGuinness et al., 1998; Vazquez-Serrano et al., 2002; Weskamp et al., 1999; Herrmann (b) et al., 1997).

Palladium and rhodium 'carbene' complexes show an excellent catalyst performance in Heck olefinations, hydroformylation, hydrogenation, and isomerization (Herrmann (a) et al., 1995; Herrmann (b) et al., 1995; Herrmann (b) et

al., 1996; Herrmann (c) et al., 1996). The metal-carbon bond of the N-heterocyclic carbene ligands is very robust so that dissociation from these metal centers (Pd, Rh) is not observed, even at elevated temperatures (Herrmann (a) et al., 1996).

In our study, X-ray datas for the crystal structure are collected with Enraf Nonius CAD-4 diffractometer, which is at X-ray Laboratory, Department of Physics Engineering, Faculty of Engineering, Hacettepe University. After this, the collected data are solved by Patterson methods with *SHELXS-86* (Sheldrick, 1990) program and the atomic parameters are refined by least squares and difference Fourier method with *SHELXL-97* (Sheldrick, 1998) program at Department of Physics, Faculty of Arts & Sciences, Dokuz Eylül University. In different steps of the study for geometrical calculations and molecular graphics; *WINGX* (Farrugia, 1999), *ORTEP* – III (Farrugia, 1997), *PLUTON* (Spek, 1990), PLATON (Spek, 1990) package programs were used. Also the chemical diagrams were formed by CHEMWIN program.

CHAPTER TWO
X-RAYS AND X-RAY DIFFRACTION DATA

2.1 X-rays

X-rays lie in the electromagnetic spectrum between ultraviolet light and gamma radiation and have an approximate range of wavelengths of 0.1-100Å. They are usually produced by rapidly decelerating fast-moving electrons and converting their energy of motion into a quantum of radiation. The wavelengths produced will depend on the energy of the electrons; we shall be concerned with X-rays having a wavelength of about 1Å. X-rays are also emitted by certain radioactive isotopes, for example, ^{55}Fe. Although such sources are convenient for testing and calibration, they have not been used for diffraction purposes.

To generate X-rays, electrons are accelerated by an electric field and directed against a metal target, which slows them rapidly by multiple collisions. Under the usual conditions most of the electrons are not brought to a full stop by a single collision, and a continuum of radiation is formed (Figure 2.1). The minimum wavelength of this **white radiation** is determined by the accelerating voltage and can be calculated from

$$\lambda_{min} = \frac{12,398}{V_{acc}}$$

$$(2.1)$$

The greatest intensity occurs at a somewhat longer wavelength. As the voltage is increased, not only are the cutoff and peak intensity moved to shorter, more

penetrating wavelengths, but also the total intensity increases even though the electron current remains the same (Stout & Jensen, 1989).
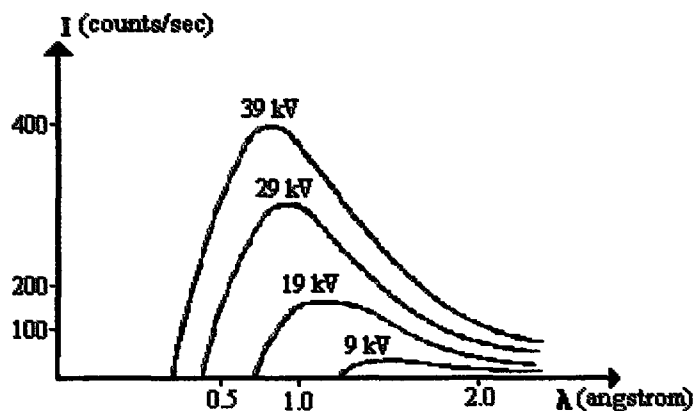
Figure 2.1 Continuous X-ray spectra as a function of accelerating voltage.

While the distribution of intensity in the white radiation depends primarily on the accelerating voltage and only to a small extent on the nature of the target material, X-ray spectra show in addition a number of sharp spikes of high intensity whose positions change from one material to another (Figure 2.2). These peaks are the **characteristic lines** for the element of which the target is made. When the electrons bombarding the target reach certain critical energies (threshold potentials) they are capable of knocking electrons out of their atomic orbitals. In particular, at energies of about 10000ev (for elements whit atomic number $\approx$ 30) they can remove electrons from the innermost (K) shell. The vacancy in the K shell is then filled by the descent of an electron from the next higher shell (L) or the one above that (M). The decrease in potential energy in going from the higher level to the lower appears as radiation, and as the energies of the shells are well defined, each transition gives a nearly monochromatic line. The principal peaks are

$$K_{\alpha 1}, K_{\alpha 2} \qquad L \rightarrow K$$
$$K_{\beta 1}, K_{\beta 2} \qquad M \rightarrow K$$
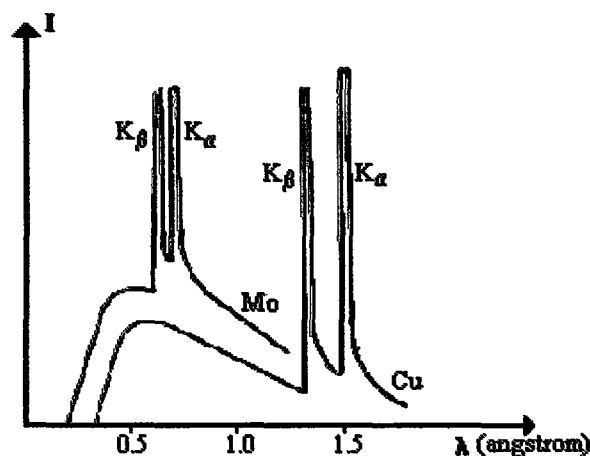
Figure 2.2 X-ray spectra for Cu and Mo target showing the characteristic lines.

Because the difference in energy between L and K is less than that between M and K, K_α is always at a longer wavelength than K_β. The lines are close doublets because transitions can occur from two possible electronic configurations, which differ slightly in energy. $K_{\alpha 1}$ is twice as intense as $K_{\alpha 2}$ and about three to six times as strong as $K_{\beta 1}$. $K_{\beta 2}$ is usually so weak that it is ignored.

As the atomic number (Z) of the target element increases, the characteristic lines shift to shorter wavelengths, and one can, in principle, select a target to give almost any desired value for the K_α line. In practice, however, one is limited to materials that are conductive, solid, dense, and high-melting, that is, to metals. Fortunately, the transition elements of the first and second long periods (Z=21-30 and 39-48) meet these requirements and have characteristic radiation in the region that is most useful for crystal structure analysis.

2.2 X-ray Diffraction

The diffraction of X-rays by crystals was discovered by Max von Laue in 1912, and the sequence of events that led to the discovery is one of the most fascinating chapters in the history of science. Although X-rays had been discovered in 1895 by Roentgen, their nature was not known. During the years following their discovery, a

number of determined efforts were made to prove them particles or waves. It was not, in fact, until diffraction by crystals was observed that their wave character was proved.

Following the experimental observation of X-ray diffraction early in 1912, von Laue showed that the phenomenon could be described in terms of diffraction from a three-dimensional grating. In the same year, however, while engaged in experimental studies, W. L. Bragg noticed the similarity of diffraction to ordinary reflection and deduced a simple equation treating diffraction as "reflection" from planes in the lattice. In order to derive the equation, we consider an X-ray beam incident on a pair of parallel planes with interplanar spacing d.
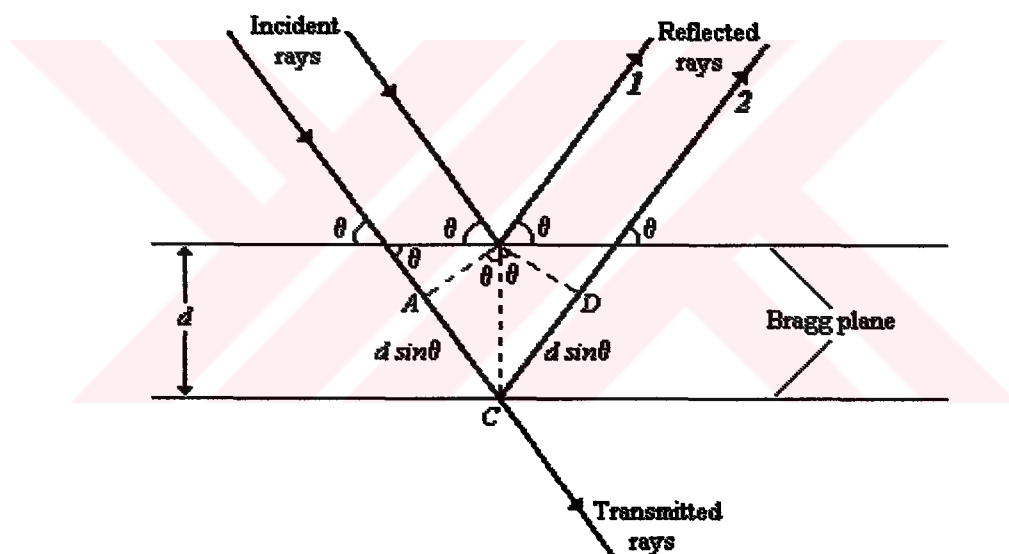
Figure 2.3 Derivation of Bragg's formula

As shown in Figure 2.3, an incident X-ray makes an angle θ with the crystal plane. If this crystal plane is a mirror plane, it is easy to show that the path difference between ray1 and ray2, $AC + CD$, is equal to $2d\sin\theta$. When it is an integral multiple n of the wavelength, we have

$$2d\sin\theta = n\lambda \qquad n = 1, 2, \dots \tag{2.2}$$

where d is the lattice spacing, λ is the incident X-ray wavelength and θ is the incident and reflected angle. The X-rays reflected in the direction θ will have a maximum in their diffraction intensity. Eqn. (2.2) is called the **Bragg Law**. When a beam of X-rays strikes a crystal, it must satisfy the Bragg Law for its reflected rays to be intensified by diffraction. From this equation we know that the wavelength must be smaller than $2d$, and, if either λ or d is known, the other can be calculated after measuring θ in a diffraction experiment (Yang & Hamilton, 1996).

2.3 Measure Methods of Diffraction Intensities

There are three well-known methods for measurement of diffraction intensities. In first of these, both crystal and detector are not moved. While crystal is constant at the reflection position, detector is constant at the 2θ position and intensity measured.

In the "w-scan" mode, the detector is held at the 2θ angle of the actual reflection and the crystal rotated on the w-axis of the diffractometer.

In the "$w/2\theta$-scan" mode, both crystal and detector are moved. The crystal is rotated by Δw, while the detector is rotated in the 2θ-circle by an angular velocity, which is twice of the crystal rotation.

The principles of "w-scan" and "$w/2\theta$-scan" methods are shown in Figure 2.4(a) and 2.4(b), respectively.
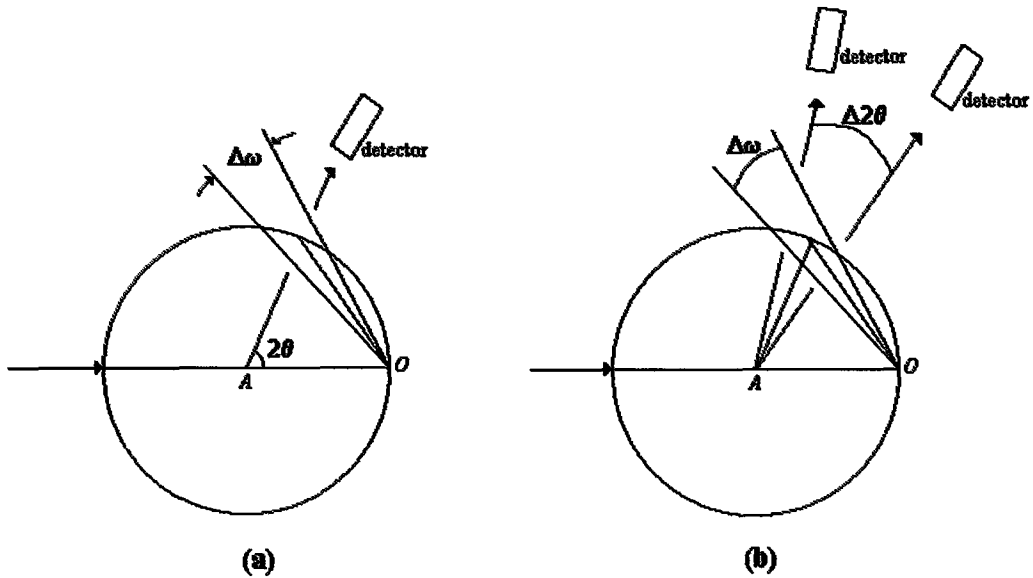
Figure 2.4 Diffractometer scan types. (a) w-scan (b) $w/2\theta$-scan

In this study, the data were collected with an Enraf-Nonius CAD-4 diffractometer. A single crystal diffractometer consist of an X-ray source, an X-ray detector, a goniometer that orients the crystal so that a chosen X-ray diffracted beam can be received by the detector, and a computer that controls (Enraf-Nonius, 1993) the goniometer and detector movements and performs the mathematical operations required to position the crystal and the detector in the desired orientations (Giacovazzo, 1998, p. 273).

2.4 Scattering of X-rays by a Crystal

When X rays are diffracted by a crystal, the intensity of scattering at any angle can be calculated by considering the combination of the waves scattered from different atoms to give various degrees of constructive and destructive interference. The waves are represented as vectors with real and imaginary components. We consider that the X-rays diffracted by structure with N atoms. The resultant of N waves is,

$$\vec{F} = f_1 e^{i\phi_1} + f_2 e^{i\phi_2} + \cdots + f_j e^{i\phi_j} + \cdots + f_N e^{i\phi_N} \tag{2.3}$$

$$\vec{F} = \sum_{j=1}^{N} f_j e^{i\phi_j} \tag{2.4}$$

On the vector representation of N waves in Figure 2.5; the resultant $\vec{F}$ is given by

$$\vec{F} = |F| e^{i\phi} \tag{2.5}$$
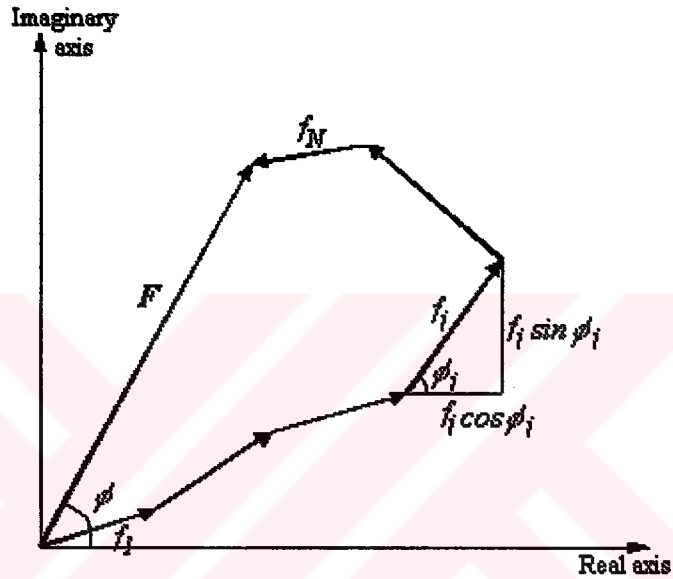
Figure 2.5 Vector Representations of N Waves

The amplitude $|F|$ is given by

$$|F|^2 = \vec{F}\vec{F}^* \tag{2.6}$$

where $\vec{F}^*$ is the complex conjugate of $\vec{F}$

$$\vec{F}^* = |F| e^{-i\phi} \tag{2.7}$$

By analogy we can write,

$$|F| = \left(A^2 + B^2\right)^{1/2} \tag{2.8}$$

where

$$A = \sum_{j=1}^{N} f_j \cos\phi_j \quad \text{and} \quad B = \sum_{j=1}^{N} f_j \sin\phi_j \tag{2.9}$$

A and B are, respectively, the real and imaginary components of $\vec{F}$, and the phase angle ϕ is given by

$$\tan\phi = \frac{B}{A} \qquad (2.10)$$

In unit cell if we consider a structure, which have fractional coordinates x_j, y_j, z_j ($j=1, 2,..., N$), the resultant of the path difference of the waves, which are scattered by j.th atom, is as follows

$$\delta_j = \lambda\left(hx_j + ky_j + lz_j\right) \qquad (2.11)$$

The phase difference can be written as

$$\Phi_j = \left(\frac{2\pi}{\lambda}\right)\delta_j \quad \text{or} \quad \Phi_j = 2\pi\left(hx_j + ky_j + lz_j\right) \qquad (2.12)$$

2.5 Crystal Structure Factor

In Eqn. (2.3), F is called *crystal structure factor*. The structure factor is the resultant of N waves scattered in the direction of the reflection *hkl* by the N atoms in the unit cell.

If we add Eqn. (2.12) into Eqn. (2.4); we can write

$$F_{hkl} = \sum_{j=1}^{N} f_j \exp\left[2\pi i\left(hx_j + ky_j + lz_j\right)\right] \qquad (2.13)$$

for crystal structure factor.

In this equation, f_j is called the atomic scattering factors. If one assumes spherical atoms, the scattering power of each atom is a function only of the atom type and $(\sin\theta)/\lambda$. It is independent of the position of the atom in the cell. The scattering power of a given atom for a given reflection is known as its *scattering*

factor (f_j) and is expressed in terms of the scattering power of an equivalent number of electrons located at the position of the atomic nucleus (Stout & Jensen, 1989, p.188).

The variation of the f_j with $(\sin\theta)/\lambda$ is shown in Figure 2.6.

$$f_j \exp(-B_{iso}\sin^2\theta/\lambda^2)$$
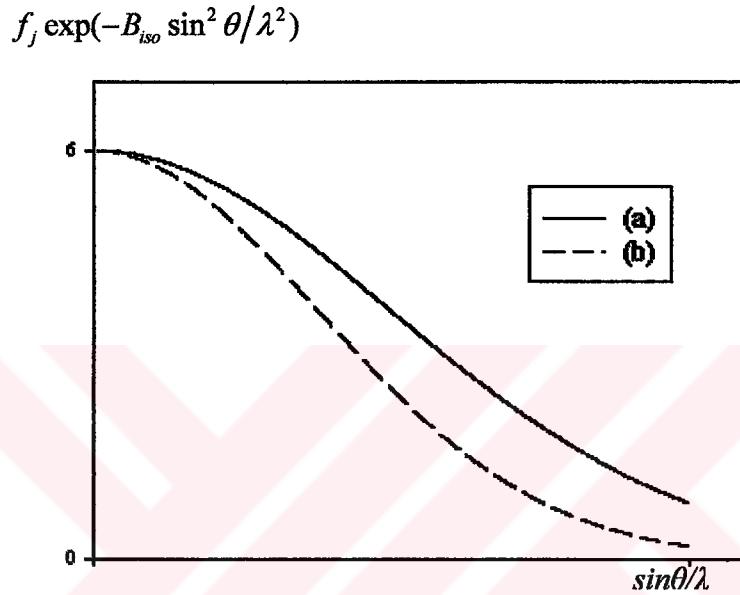
Figure 2.6 Atomic scattering factors: (a) stationary atom, (b) atom corrected for thermal vibration.

2.6 Fourier Synthesis and Electron Density

The electron distribution around the atoms is presented electron density function. In crystal, atoms have three-dimensional periodic order. Because of this, the number of electrons per unit volume or electron density at x, y, z point in crystal, can be shown with three dimensional Fourier series

$$\rho(x,y,z) = \frac{1}{V} \sum_{h,k,l=-\infty}^{+\infty} F(hkl)\exp[-2\pi i(hx+ky+lz)] \tag{2.14}$$

In this equation, V is volume of unit cell, *F(hkl)* is structure factor. From (2.5), Φ(hkl) phases angle of a crystal structure factor;

$$\Phi(hkl) = \arctan\left[\frac{B(hkl)}{A(hkl)}\right]$$ (2.15)

can be written. Fridel law proved that diffraction patterns have a center of symmetry,

$$F(hkl) = F(\overline{hkl}) \qquad \text{or} \qquad \Phi(\overline{hkl}) = -\Phi(hkl)$$ (2.16)

and electron density function can be written as

$$\rho(x,y,z) = \frac{1}{V}\sum_{h,k,l=-\infty}^{+\infty} F(hkl)\exp i[2\pi(hx+ky+lz) - i\Phi(hkl)]$$ (2.17)

If we write this equation as trigonometric function, the electron density as follows

$$\rho(x,y,z) = \frac{1}{V}\sum_{h,k,l=-\infty}^{+\infty} |F(hkl)|\cos[2\pi(hx+ky+lz) - \Phi(hkl)]$$ (2.18)

As we can see at top equation, if we knew $|F(hkl)|$ and $\Phi(hkl)$ we could compute ρ for all values of x, y, z and plot the values obtained to give a three-dimensional electron density map. Then, assuming atoms to be at the centers of peaks, we would know the structure. But the experimental measured diffraction intensities give us only amplitudes of crystal structure factors. So we need the phases, $\Phi(hkl)$, for three dimensional electron density map.

In this study, **Patterson method** has been used in order to derive the phases.

2.7 Data Reduction

Intensity data constitute the raw material from which crystal structures are derived. In most cases they represent all the information that will be obtained from physical measurements on the crystal, and the subsequent development of a structure will depend on the skillful extraction of the information contained within the intensities. It is the preliminary manipulation of these intensities; their conversion to a corrected, more generally usable form, which is referred to as **data reduction**; with which we shall deal in this chapter.

Structure factor is related to the experimentally observed intensities

$$I(hkl) \approx |F(hkl)|^2 \qquad (2.19)$$

It is need to add some corrections on this proportional in order to transform this ratio. Exact ratio shown that;

$$I(hkl) = K.L.p.T.A.E.|F(hkl)|^2 \qquad (2.20)$$

K: Scale factor

L: Lorentz factor

p: Polarization factor

T: Debye-Waller Temperature factor

A: Absorption factor

E: Extinction factor

2.7.1 Lorentz Correction

We have seen that diffraction arises whenever reciprocal lattice nodes, that always have a non-negligible volume, cross the sphere of reflection. If a node is in diffracting position for a longer time, the intensity of the corresponding reflection will be proportionally higher. This factor would not be important if the method used to record the integrated intensities ensured that every reciprocal lattice node were in a

diffracting position for exactly the same time, as it would effect every reflection in the same way and in the end it would simply scale all the intensities by the same factor. This, however, is not the case. Depending on the method used to record the reflection intensity and on the position of the reciprocal lattice node, the times required for different nodes to cross the Ewald sphere are different. The Lorentz correction simply takes this factor into account.

The time a node is in diffracting position is dependent on two factors. The position of the node and the velocity with which it sweeps through the sphere of reflection. We will derive the form of the Lorentz factor in a very simple case and then show the form it takes in a more complicated situation (Giacovazzo, et al., 1998).
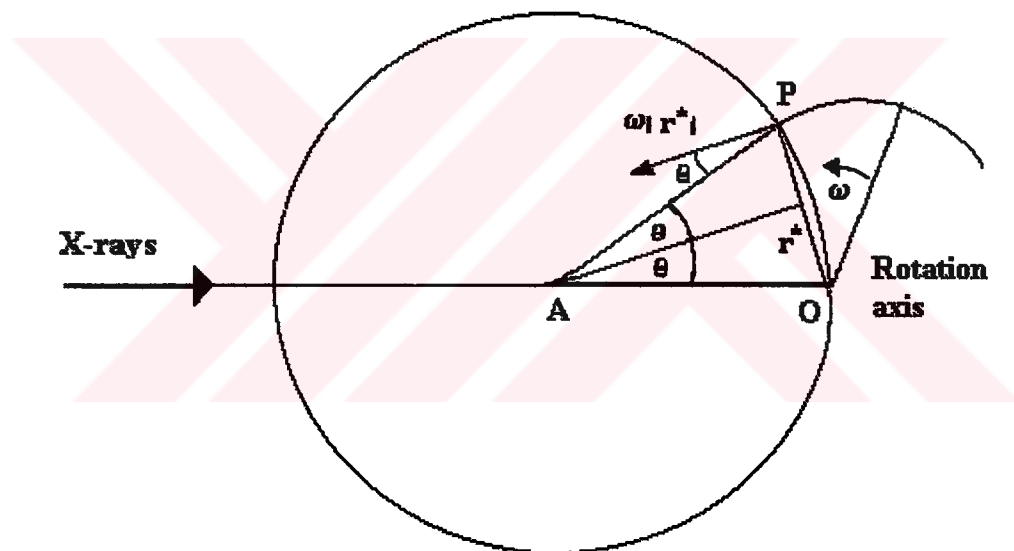
Figure 2.7 Ewald sphere

Figure 2.7 shows the Ewald sphere for a diffraction experiment in which the crystal is rotated about an axis which is normal to the plane defined by the incident and the diffracted beams. This is for example the case of a zero-level rotation or Weissenberg photograph or of the equatorial reflections measured with a diffractometer.

The crystal, and therefore the reciprocal lattice, is assumed to be rotated at a constant angular velocity ω; if V_n is the linear velocity component of the reciprocal lattice node along the radius of the sphere of reflection, the Lorentz factor can be defined as follows;

$$L = \frac{w}{V_n \lambda} \tag{2.21}$$

Which is indeed proportional to the time during which diffraction takes place for a given reciprocal lattice node.

The linear velocity of the point P is

$$V = |r^*| w \tag{2.22}$$

and its component along the radius of the Ewald sphere

$$V_n = |r^*| w \cos\theta \tag{2.23}$$

Since θ is the angle formed by the linear velocity V and the radius of the sphere of reflection passing through the point P as shown in Figure 2.7. Substituting $|\ r^*\ |$ in terms of Bragg's law

$$r^* = \frac{1}{d} = 2\sin\theta / \lambda \tag{2.24}$$

$$V_n = (w/\lambda)2\sin\theta\cos\theta \tag{2.25}$$

And

$$L = (\sin 2\theta)^{-1} \tag{2.26}$$

Which is the simplest possible form that can be taken by the **Lorentz factor**.

2.7.2 Polarization Correction

The polarization correction depends on the state of polarization of the incident X-ray beam and on the scattering angle of the diffracted beam. When a totally non-polarized beam is diffracted by a crystal, the diffracted intensity is affected by a factor, called the polarization factor, which in this simple case was shown to be equal to

$$p = \frac{1}{2}\left(1 + \cos^2 2\theta\right) \tag{2.27}$$

where θ is the Bragg angle of the reflection considered and the diffracting crystal was tacitly assumed to be ideally mosaic. This simple expression for the polarization correction can be applied whenever the incident X-rays are not polarized, that is when the radiation is produced by a conventional source and monochromatized using an appropriate filter.

2.7.3 Absorption Factor

The intensity of the diffracted X-rays is thus reduced, with respect to what it would be without absorption by the factor

$$\frac{I}{I_0} = \exp(-\mu x) \tag{2.28}$$

Which is valid for every point in the crystal. Here x is the total path length and μ is the linear absorption coefficient, in this case, of the crystal.

Eqn. (2.28) can be used to calculate a very rough estimate of the optimum crystal size for a given compound of linear absorption coefficient μ.

The linear absorption coefficient for the crystal can be calculated from the mass absorption coefficients of the atoms present in the unit cell. No structural knowledge is required, only the values of the mass absorption coefficients of the elements which can be found in the international tables for X-ray crystallography. From the values of μ_m for a given wavelength, μ can be calculated by the following equation;

$$\mu = \rho \sum_i g_i \mu^i_m \tag{2.29}$$

where g_i is the mass fraction of element i present in the unit cell, μ^i_m is its mass absorption coefficient, and ρ is the crystal density. Recall that μ^i_m is a function of the atomic number of the element and of the wavelength of the radiation used. It is smaller for lower atomic numbers and for shorter wavelengths. This explains why absorption corrections become more important for heavy-element crystals and for radiation of longer wavelengths. Sometimes all it takes is a change from copper to molybdenum radiation to sufficiently reduce the absorption problem in a given crystal structure determination. In any case it is always instructive to calculate the value of μ for the crystal being examined in order to get an indication of the severity of the absorption problem (Giacovazzo et al., 1998, pp. 304).

Table 2.1 Atomic mass and mass absorption coefficients for $C_{27}H_{34}N_2O_4ClRh$.

Atom	Number of Atoms	Atomic mass (akb)	Total Mass (akb)	Percent in compound	Mass absorption coefficient (MoK_α)
C	27	12.01	324.27	55.1	0.70
H	34	1.01	34.34	5.8	0.37
N	2	14.01	28.02	4.8	1.10
O	4	16.00	64.00	10.9	1.50
Cl	1	35.45	35.45	6.0	11.62
Rh	1	102.90	102.90	17.5	25.3

$$\sum_i m_i = 588.98 \text{ akb}, \quad \rho = 1.53 \, g/cm^3, \quad \mu = \rho \sum_i g_i \mu^i_m = 0.880 \, mm^{-1}$$

The linear absorption coefficient is found $\mu = 0.880 \, mm^{-1}$ for our crystal.

2.7.4 Debye-Waller Temperature Factor Correction

Thermal motion also has an effect on the X-ray intensities. The normal scattering factor curves are calculated on the basis of the electron distribution in a stationary atom, but in fact the atoms in crystals are always vibrating about their rest points. The magnitude of the vibration depends on the temperature, the mass of the atom, and the firmness with which it is held in place by covalent bonds or other forces. In general, the higher the temperature, the greater the vibration. The effect of such *thermal motion* is to spread the electron cloud over a larger volume and thus to cause the scattering power of the real atom to fall off more rapidly than that of the ideal, stationary model. It has been shown both theoretically and practically that the change in scattering power can be given by the expression (Stout & Jensen, 1989)

$$\exp\left(-B\frac{\sin^2\theta}{\lambda^2}\right) \qquad (2.30)$$

where B is related to the mean-square amplitude $\overline{\left(u^2\right)}$ of atomic vibration by

$$B = 8\pi^2\overline{u^2} \qquad (2.31)$$

Thus the proper scattering factor for a real atom is not simply f_0, but rather the combined expression

$$f = f_o\exp\left(-B\frac{\sin^2\theta}{\lambda^2}\right) \qquad (2.32)$$

where f_o is scattering amplitude at $0\ K$ and f is scattering factor at laboratory temperature. After the Lorentz-polarization $(L-p)$ correction is done, an average observed intensity becomes

$$\overline{I_{obs}} = \left\langle\left|F_{obs}\right|^2\right\rangle_{ave} \qquad (2.33)$$

For a unit cell that contains N atoms, it can be shown fairly easily that the theoretical average intensity is given by

$$\overline{I_{cal}} = \sum_{i=1}^{N}f_i^2 \qquad (2.34)$$

If we unite (2.32) and (2.34),

$$\overline{I_{obs}} = \sum_{i=1}^{N} f_{oi}^2 \exp\left(-B\frac{\sin^2\theta}{\lambda^2}\right) \tag{2.35}$$

here B is constant for all atoms and can be calculated. Than, we can write

$$\overline{I_{obs}} = \exp\left(-B\frac{\sin^2\theta}{\lambda^2}\right)\sum_{i=1}^{N} f_{oi}^2 \tag{2.36}$$

Now if

$$\overline{I_{cal}} = C\overline{I_{obs}} \tag{2.37}$$

$$\overline{I_{cal}} = C\exp\left(-B\frac{\sin^2\theta}{\lambda^2}\right)\sum_{i=1}^{N} f_{oi}^2 \tag{2.38}$$

and taking the natural logarithm of both sides,

$$\ln\left[\frac{\overline{I_{cal}}}{\sum_{i=1}^{N} f_{oi}^2}\right] = \ln C - \left[2B\frac{\sin^2\theta}{\lambda^2}\right] \tag{2.39}$$

Thus if the left side of (2.39) is evaluated for each of the shells of constant f, and the values are plotted against $(\sin^2\theta)/\lambda^2$, the result should be a straight line in which the extrapolated intercept at $(\sin^2\theta)/\lambda^2 = 0$ is ln C and the slope is $-2B$. B can thus be obtained directly from the slope, and C is related to the scale constant k needed to convert $|F_{cal}|$ to $|F_{obs}|$ by

$$k = \frac{1}{\sqrt{C}} \tag{2.40}$$

where

$$|F_{obs}| = k|F_{cal}| \tag{2.41}$$

$$\ln \frac{\overline{I_{cal}}}{\sum_{i=1}^{N} f_{oi}^2}$$

$$\ln C$$

$$slope = (-2B)$$

$$\frac{\sin^2 \theta}{\lambda^2}$$
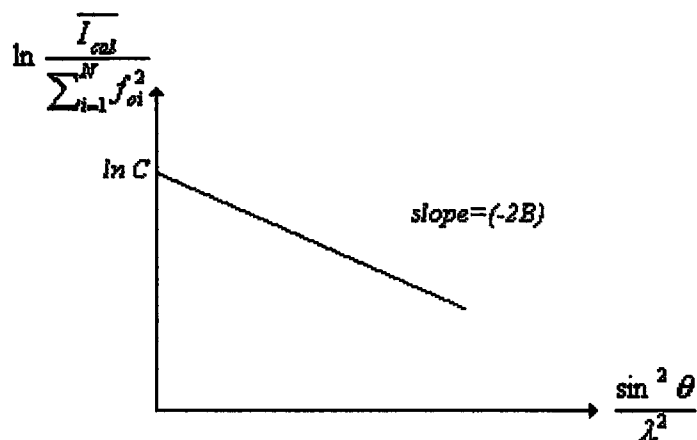
Figure 2.8 Wilson plot.

2.7.5 Extinction Correction

E is the extinction coefficient. It depends on the mosaic structure of the crystal and has two components. The most important one, called **secondary extinction**, takes into account the fact that the lattice planes first encountered by the primary beam will reflect a significant fraction of the primary intensity so that deeper planes receive less primary radiation. That causes a weakening of the diffracted intensity, mainly observable for high-intensity reflections at low $(\sin\theta)/\lambda$ values in sufficiently perfect crystals. If the mosaic blocks are misoriented (as they usually are) then they do not diffract together and shielding of deeper planes is consequently reduced. Secondary extinction is equivalent to an increase of the linear absorption coefficient: thus it is negligible for sufficiently small crystals. Reflections affected by secondary extinction can be recognized in the final stages of the crystal structure refinement when for some high-intensity reflection $|F_{obs}| < |F_{cal}|$ (Giacovazzo et al., 1998).
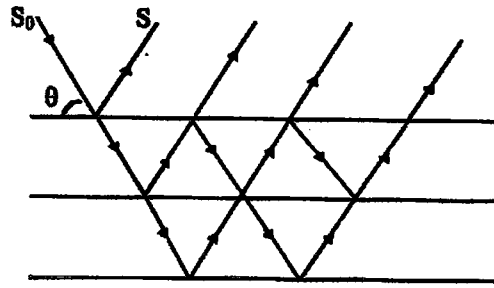
Figure 2.9 Multiple reflections from a family of lattice planes.

The second component of the extinction coefficient, called **primary extinction,** takes into account the loss of intensity due to dynamic effects inside every single block. This phenomenon can be understood intuitively by means of Figure 2.9. At the Bragg angle every incident wave can suffer multiple reflections from different lattice planes: after an odd number of reflections the direction will be the same as the diffracted beam: after an even number of reflections the direction will be the same as the primary beam. Each scattering causes a phase lag of $\lambda/4$. Thus, the unscattered radiation having direction S_0 in Figure 2.9 is joined by doubly scattered radiation (with much smaller intensity) with a phase lag of π : consequently destructive interference will result. The same consideration holds for waves propagating along the direction of the diffracted beam: the result is that both primary and diffracted beams are weakened because of dynamical effects.

.

2.7.6 Anomalous Scattering Factor

It is well known that electrons are bound to the nucleus by forces which depend on the atomic field strength and on the quantum state of the electron. Therefore they have to be considered as oscillators with natural frequencies. If the frequency of the primary beam is near to some of these natural frequencies resonance will take place. The scattering under these conditions is called anomalous and can be analytically expressed by substitution of the atomic scattering factor f_a defined earlier by a complex quantity

$$f = f_a + \Delta f' + if'' = f' + if'' \qquad (2.42)$$

$\Delta f'$ and f'' are called the real and imaginary dispersion corrections.

It is clear that for a noncentrosymmetric structure Fridel's law does not hold and that $\Phi(hkl) \neq -\Phi(\overline{hkl})$. If the scattering factors are not handled properly, dispersion introduces error. This can be minimized, however, by an appropriate choice of radiation (Stout & Jensen, 1989).

CHAPTER THREE

SOLUTION OF CRYSTAL STRUCTURES

3.1 Phase Problem

If we remember Eqn. (2.18), the electron density at a point x, y, z in a unit cell of volume V is

$$\rho(x,y,z) = \frac{1}{V} \sum_{h,k,l=-\infty}^{+\infty} |F(hkl)| \cos[2\pi(hx + ky + lz) - \Phi(hkl)] \qquad (3.1)$$

Therefore if we knew $|F(hkl)|$ and $\Phi(hkl)$ we could compute ρ for all values of x, y, z and plot the values obtained to give a three-dimensional electron density map. Then, assuming atoms to be at the centers of peaks, we would know the entire structure. However, we can usually obtain only the structure factor amplitudes $|F(hkl)|$ and not the phase angles, Φ, directly from experimental measurements. We must usually derive Φ, either from values of A and B computed from structures we have guessed or by purely analytical methods. This is the **phase problem.**

Approximations to electron density maps can be calculated with experimentally observed values of $|F(hkl)|$ and values of Φ derived from a trial structure. If the trial structure is not too grossly in error, the map will be a reasonable representation of the correct electron density map.

3.2 Direct Methods

With the term *direct methods* are the methods which try to derive the phases of a set of structure factors directly from the magnitudes through mathematical relationships. These magnitudes are calculated readily from the observed intensities, knowledge of the size and symmetry of the unit-cell, and the chemical composition of the substance being studied. In the case of X-ray diffraction, it is possible to relate the phase and the amplitude of a wave, two important properties of the electron density function should be considered:

1. It is everywhere positive, $\rho(\vec{r}) \geq 0$ (positivity);

2. It is composed of discrete atoms (atomicity).

Historically the first mathematical relationships capable of giving phase information were obtained, in the form of inequalities, by Harker and Kasper and by Gillis in the late 1940s and early 1950s. Some of these inequalities provided unambiguous phase relationships for the centrosymmetric decaborane structure, with Harker and Kasper solved with their aid, but the Harker-Kasper approach had no great impact initially, because it was limited in practice to rather simple centrosymmetric structures. Gillis made the important point that, even when the inequalities could not define the sign of a particular structure factor, they might imply a sign if the inequality was nearly satisfied. The next important advance was by Karle and Hauptman in 1950, dealing again with inequalities but in a more general and eventually fruitful way. They showed that inequalities restrict the range of phase angles for a non-centrosymmetric structure (Lecture notes, 2001).

In 1953 Sayre considered that for a structure formed by well resolved and almost equal atoms, the two functions $\rho(\vec{r})$ and $\rho^2(\vec{r})$ are quite similar and show maxima at the same positions. A one-dimensional example is illustrated in Figure 3.1. Cochran, and independently Zachariasen, arrived at relations among the signs of structure factors of three related reflections, relations that were shown to have a high probability of being valid. The relation among the indices of any three reflections was that the indices of one of them must be expressible as the sum of the indices of

the other two. The relation was called a triple-product sign relationship, or *TPSR*, because if we let *H* represent a reflection *(h, k, l)*, *K* represent *(h', k', l')*, and *s* be "the sign of the structure factor of", then the product of the signs of *H*, *K* and *(H+K)* is very likely to be positive:

$$s(H).s(K).s(H+K) \approx + \qquad (3.2)$$
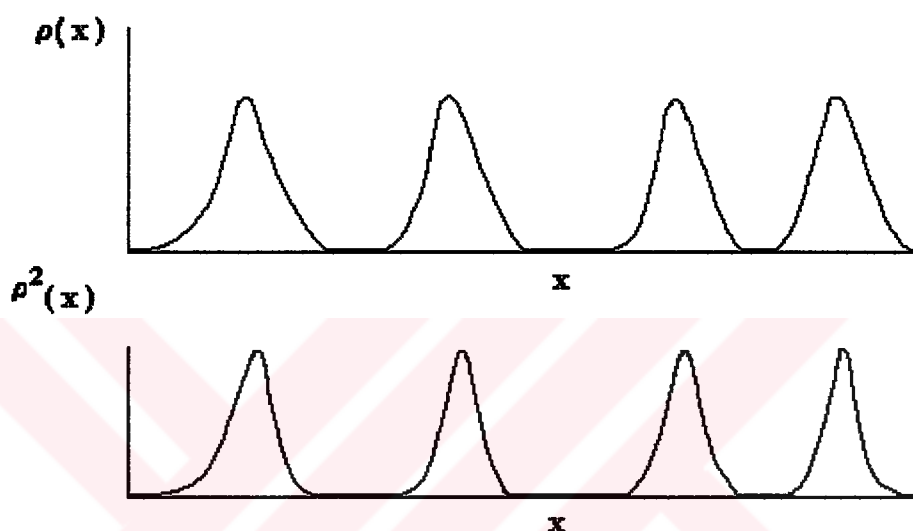
Figure 3.1 Comparison between $\rho(x)$ and $\rho^2(x)$ for a one-dimensional structure with equal and well resolved atoms.

It turns out that, for most structures, one needs good approximations to the phases of only about 10 percent of the observed reflections to get a recognizable picture of the structure from an "E-map", which is a three-dimensional Fourier synthesis calculated with $E(hkl)$ rather than $F(hkl)$. Because the method is successful even when there are some errors in the initial phases, it is not necessary in applying direct methods that all the assumptions made in deriving the equations used be fulfilled exactly. The errors in phases are reduced as the image of the molecule is improved through successive E-maps and F-maps, and as refinement proceeds by least-squares or other methods are used.

Many people contributed to the development of direct methods, but the key significance of the contributions of Herbert Hauptman and Jerome Karle was recognized by the award to them of the Nobel Prize for Chemistry in 1985.

3.3 Patterson Methods

3.3.1 Introduction to the Patterson Methods

$$P_{xyz} = \frac{1}{V}\sum |F_{hkl}|^2 \cos 2\pi(hx + ky + lz), \text{ summed over all reflections} \quad (3.3)$$

If the crystallographic Fourier calculation is made using F^2 values as the coefficients it will produce a three dimensional map with peaks which represent not atoms but inter-atomic vectors. The value of such a map for deducing atoms positions to initiate a trial structure was first described by A. L. Patterson in 1935, ergo terms such as "Patterson" maps, "Patterson" summations, and "Patterson" methods. Until the development of the direct method the Patterson method was dominant approach for starting structures, and is still used for organometallic complexes and macromolecular structures (Lecture Notes, 2001).

The salient points about Patterson maps are:
  a) Each peak on the Patterson map represents a vector from the origin to that peak, and this vector corresponds to a vector between two atoms.
  b) For n total atoms in the cell there are n^2 peaks on the Patterson map. Since n of these are at the origin (see below) there are $(n^2 - n)$ non-origin vectors.
  c) Peak heights are approximately proportional to the product of the atomic numbers of the two atoms that produce that peak. Thus, in a structure containing Ru and C, the Ru-Ru, Ru-C, and C-C vectors have relative peak heights of roughly.
  d) Patterson peak widths are greater than those of electron density maps.
  e) The always-large origin peak corresponds to the sum of vectors between each atom and itself.

f) The Patterson has the same unit cell and the same translational symmetry (centering) as the crystal.
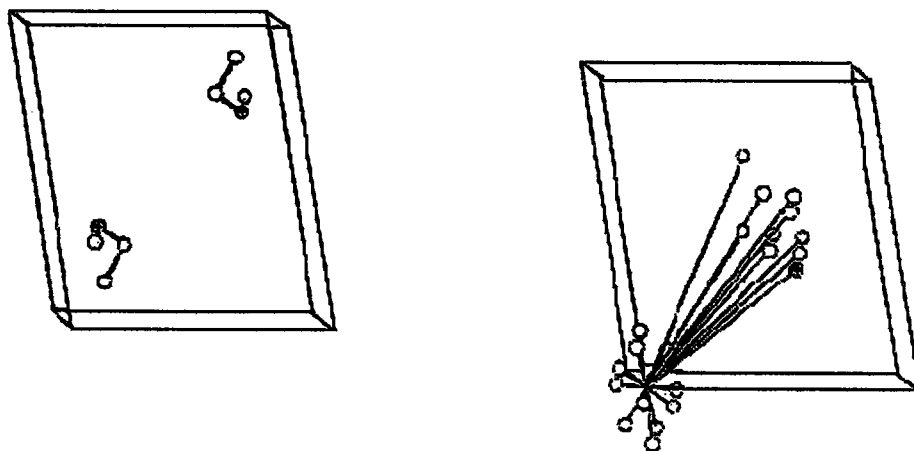
Figure 3.2 The figures up illustrate the relationship between the atoms in a cell (left figure) and the peaks on a Patterson map (right figure).

3.3.2 Patterson Symmetries

Before illustrating the methods for interpreting the Patterson function, let us first analyse how the **symmetry** of the crystal is reflected into the vector map. The following considerations apply:

1. All Patterson functions are centrosymmetric, regardless of the space group of the atomic distribution from which it is derived.
2. Their lattice type (P, C, F, etc.) is the lattice type of the original space group.
3. Their space group is derived from the original space group by replacing all translational symmetry elements (screws, glides) by the corresponding nontranslational elements (axes, mirrors) and by adding a center of symmetry if it is not already present (Stout & Jensen, 1989, p. 284).

The following table gives the Patterson symmetries for the primitive space groups.

Table 3.1 Patterson symmetries for the primitive space groups

Space Groups	Space Group of the Vector Map
Triclinic	P-1
Monoclinic	P2/m
Orthorhombic	Pmmm
Tetragonal	P4/m
Tetragonal	P4/mmm
Trigonal	P-3
Trigonal	P-3m1
Hexagonal	P 6/m
Hexagonal	P6/mmm
Cubic	Pm3
Cubic	Pm3m

For A-, C-, F-, I-, and R-centered cells the relationships parallel those given for the primitive groups above. For example: All I-centered orthorhombic cells have vector maps in space group Immm; C-centered monoclinic cells have vector symmetry C2/m; and the centered space group F-43m has a vector map in space group Fm3m parallel to space group P-43m having a vector map in space group Pm3m (Lecture Notes, 2001).

3.3.3 Locating One Heavy Atom

If the structure of interest contains only one heavy atom per formula unit, the location of that atom is usually straightforward. A general list of vectors between the heavy atoms is obtained by a simple hand calculation.

Table 3.2 Examples of locating an atom at different space groups

| | For P-1 (Z=2) | | | For P2₁/n (Z=4) | | | For Pna2₁ (Z=4) | |

For P-1 (Z=2):

	x	*y*	*z*
x y z	0	0	0
-x -y -z	2x	2y	2z

For P2₁/n (Z=4):

	x	*y*	*z*
x y z	0	0	0
-x -y -z	2x	2y	2z
.5-x .5+y .5-z	.5+2x	.5	.5+2z
.5+x .5-y .5+z	.5	.5+2y	.5

For Pna2₁ (Z=4):

	x	*y*	*z*
x y z	0	0	0
-x -y, .5+z	2x	2y	.5
.5-x .5+y .5+z	.5+2x	.5	.5
.5+x .5-y z	.5	.5+2y	0

In these three examples the italicized x, y, z's at the top and the left side of the boxes are atom positions. The positions in bold type within the box are the vectors obtained by subtracting the left-column entries from the x, y, z atom position.

With this work done, it is usually a simple process to match the intense Patterson peaks with the vector expressions in the boxes above. Vectors which occur on special "lines" or planes (involving special values such as 0.0 or 0.5 for x, y and or z) are called *Harker peaks*, and the assignments usually start with these peaks because they are easiest to recognize and because they are generally, by reasons of symmetry, more intense.

If the most intense non-origin peak on a P −1 Patterson map is at 0.44, 0.16, 0.68, this is likely the 2x, 2y, 2z peak for the heavy atom and gives the atom position of 0.22, 0.08, 0.34. A very fast start of the trial structure. (Note that if the x value for the vector is taken as the equivalent values of 1.44 or −0.56 instead of 0.44, the x for the atom position would be 0.72 which is a harmless shift of origin by 0.5 in x; the same holds for y and z).

Similarly, consider a Patterson map of a heavy-atom structure in P2₁/n which has two Harker peaks of high intensity at (a) 0.50, 0.88, 0.50 and (b) 0.36, 0.50, 0.84. Because of the 0.5 patterns, (a) looks like the expected 0.5, 0.5+2y, 0.5 Harker peak, giving y= 0.19, and (b) looks like expected 0.5+2x, 0.5, 0.5+2z Harker peak, giving

x =0.43 (or -0.07) and z= 0.17. Thus the heavy atom is at 0.43, 0.19, 0.17 and its 2x, 2y, 2z peak is expected at 0.86, 0.38, 0.34.

Note on the table above that none of the Patterson peaks for the space group Pna2$_1$ give any information about the z coordinate of the heavy atom. The formulas for the four atom positions show that this is a polar space group with a "floating z"; the z of the first atom is arbitrary and establishes the origin in the z direction.

3.3.4 Locating Two Independent Heavy Atoms

The simple approach used in the last section for a single heavy atom can sometimes be extended to a structure with more than one independent heavy atom. As an example, assume there are two independent heavy atoms in space group P-1.

Table 3.3 An example on locating two independent heavy atoms

	x y z	x' y' z'
x y z -x -y -z	0 0 0 2x 2y 2z	Δx Δy Δz Σx Σy Σz
x' y' z' -x' -y' -z'	Δx Δy Δz Σx Σy Σz	0 0 0 2x' 2y' 2z'

If one is at x, y, z and the other at x', y', z', the vector calculation becomes, where Δx = x - x', Δy=y - y', Δz= z - z', Σx = x + x', Σy= y + y', and Σz =z + z'

As seen, the Δ and Σ vectors are double-weighted and thus should be the most intense peaks on the Patterson map. Note the sum of the Σ vector and the Δ vector equals the 2x2y2z vector [(x+x')+(x-x')=2x], and the difference of the Σ vector and the Δ vector equals the 2x'2y'2z' vector [(x+x')-(x-x')=-2x']. If the above set of four

vectors can be identified the coordinates of the xyz atom can be obtained by halving 2x2y2z, which also fixes the origin for the structure. Halving 2x'2y'2z' gives a 2-fold uncertainty for each of x', y' and z' in that 0.5 can be added to any calculated value. Adding either the Σ or Δ vector and its inverse to xyz and checking the results with the 2x'2y'2z' vector will remove this uncertainty.

3.3.5 Patterson Search and Superposition Methods

Superposition Methods: There are several methods, often quite powerful, for finding the structure corresponding to Patterson maps by transcribing P_{xyz} upon itself with different relative origins (but always the same orientation). One of the simplest methods of analyzing the Patterson map of a compound containing an atom in a known position is to calculate, graphically or by computer, a vector superposition map.

The origin of the Patterson map is put, in turn, at each of the symmetry-related positions of the known atom and the values of P_{xyz} are noted at all points in the unit cell. The *lowest value* of P in the different superposed Patterson maps is recorded for each point; the resulting distribution is called a *minimum function*. The principle underlying this approach is that it isolates the vectors arising from the interaction of the known atom with all other atoms in the structure. At points corresponding to the positions of atoms there will be peaks in the minimum function, each corresponding to a peak in each Patterson map at this position as the origin was moved. In some of the maps there will be other peaks at this same position, corresponding to other vectors in the structure, but these *accidental* superpositions are eliminated if the minimum value of P in all the superposed maps is recorded. This method is increasingly powerful when the position of more than one atom is known initially (Glusker & Trueblood, 1972, pp. 86).

Search Methods: Systematic Patterson search methods were developed for small molecule structures and are used for macromolecular structures. If the dimensions of a molecule or part of a molecule in a crystal structure are known, but its orientation (and position) in the unit cell is unknown, the *orientation* may often be found by a comparison of calculated and observed vector maps around the origin.

The fit of the calculated and observed Patterson maps can be optimized with a computer by making a "rotational search" to examine all possible orientations of one map with respect to the other and to assess the degree of overlap of vectors as a function of the angles through which the Patterson map has been rotated. The maximum overlap normally occurs (except for experimental errors) at or near the proper values of these rotation angles, thus giving the approximate orientation of the group. Then the Patterson map can be searched for vectors between groups in symmetry-related positions, and the exact position of the group in the unit cell can be found and used as part of a trial structure.

CHAPTER FOUR
CRYSTAL REFINEMENT

4.1 Introduction

After approximate positions have been determined for most, if not all, of the atoms, refinement of the structure can be started. The atomic parameters that were determined with Direct, Patterson or other methods can be refined. Additional atoms can be located and their parameters also refined. These additional atoms are found using the Fourier synthesis method.

Two methods have been used for the refinement of the atomic positions and displacement (or temperature) parameters. One method is based on Fourier techniques, so called *Difference Fourier Method*, and the other is based on least-squares techniques, so called *Least-Squares Method*.

4.2 Least Squares Method

The principle of least squares method is that minimizes the sums of the squares of differences between the observed and calculated structure factors in order to increase the sensitive of atomic parameters.

We can write the calculated structure factor, for a better set of atomic coordinates and temperature factors,

$$F_{cal}(hkl) = \sum_{j=1}^{N/2} 2f_j \exp\left(-B_j \frac{\sin^2 \theta}{\lambda^2}\right) \cos 2\pi(hx_j + ky_j + lz_j) \qquad (4.1)$$

where the structure is centrosymmetric and the temperature factor is isotropic. The correct values of parameters for j.th is as follows :

$$(B_j + \Delta B_j, x_j + \Delta x_j, y_j + \Delta y_j, z_j + \Delta z_j) \qquad (4.2)$$

and experimental (observed) structure factor can be written as (Aygün, 1997)

$$F_{exp}(hkl) = \sum_{j=1}^{N/2} 2f_j \exp\left\{-(B_j + \Delta B_j)\frac{\sin^2\theta}{\lambda^2}\right\} \cos 2\pi \left\{\begin{array}{l} h(x_j + \Delta x_j) + k(y_j + \Delta y_j) \\ + l(z_j + \Delta z_j) \end{array}\right\}$$

$$(4.3)$$

The difference of two expressions

$$\Delta F(hkl) = F_{exp}(hkl) - F_{cal}(hkl) \qquad (4.4)$$

and $\Delta F(hkl)$ can be written as

$$\Delta F_{hkl} = \sum_{j=1}^{N/2}\left[\frac{\partial(F_{cal})_{hkl}}{\partial B_j}\Delta B_j + \frac{\partial(F_{cal})_{hkl}}{\partial x_j}\Delta x_j + \frac{\partial(F_{cal})_{hkl}}{\partial y_j}\Delta y_j + \frac{\partial(F_{cal})_{hkl}}{\partial z_j}\Delta z_j\right] \qquad (4.5)$$

In order to the best approximation for observed structure factors, the following expression must be minimum.

$$R_s = \sum_h \left\{(F_{exp})_h - (F_{cal})_h\right\}^2 \approx 0 \qquad (4.6)$$

4.3 Difference Fourier Method

Another convenient way of completing refining a structural model is the **difference Fourier synthesis method.** In this method, we investigate the difference between experimental and calculated electron densities. Calculated electron density is shown,

$$\rho_{cal}(\vec{r}) = \frac{1}{V} \sum_{hkl} F_{cal}(hkl) \exp(-2\pi i \vec{h}.\vec{r}) \tag{4.7}$$

experimental electron density is shown,

$$\rho_{exp}(\vec{r}) = \frac{1}{V} \sum_{hkl} F_{exp}(hkl) \exp(-2\pi i \vec{h}.\vec{r}) \tag{4.8}$$

In order to see how much the initial model deviates from the real structure, the difference series,

$$\Delta\rho(\vec{r}) = \rho_{exp}(\vec{r}) - \rho_{cal}(\vec{r}) = \frac{1}{V} \sum_{hkl} \left[F_{exp}(hkl) - F_{cal}(hkl) \right] \exp(-2\pi i \vec{h}.\vec{r}) \tag{4.9}$$

If in the model an atom is missing, then $\rho_{cal}(\vec{r})$ will be zero at the corresponding position, while $\rho_{exp}(\vec{r})$ will show a maximum. The difference synthesis will also show a peak at the same position but it will be almost zero at the positions of model atoms where $\rho_{exp}(\vec{r}) \approx \rho_{cal}(\vec{r})$.

4.4 Error Analysis

4.4.1 R Factors

The most important factor in crystallography is known **reliability factor**. This factor denotes how well the calculated model fits the observed data and can be written as

$$R = \frac{\sum_{hkl} \left(\left| |F_{exp}(hkl)| - |F_{cal}(hkl)| \right| \right)}{\sum_{hkl} \left(|F_{exp}(hkl)| \right)} \tag{4.10}$$

The lower the value of R, the greater the confidence that can be placed in the calculated structure. Although at the beginning of refinement R factor takes big values as 0.4, 0.5, at the end of the refinement R factor takes small values then 0.06.

Another factor in crystallography is known **weighted R-factor**. In this factor, some big false reflections refining and approach to the best real structure.

Weighted R- factor is shown,

$$R_w = \sqrt{\frac{\sum_{hkl} w\{|F_{exp}(hkl)| - |F_{cal}(hkl)|\}^2}{\sum_{hkl} w\{|F_{exp}(hkl)|\}^2}}$$

(4.11)

In this equation w is weighting function. For w=1, all reflections takes equal weight. In structure solving process, various weighting functions are used (Aygün, 1997).

Weighted R- factor (R_w) can be takes a little big value than reliability (R) factor.

4.4.2 Goodness of Fit

Another index obtained from the least-squares refinement is the "**Goodness of fit**",

$$Goof = S = \sqrt{\frac{\sum_{hkl} w\{F_{exp}^2(hkl) - F_{cal}^2(hkl)\}^2}{(n-p)}}$$

(4.12)

In this equation, n is reflection number in refinement period and p is total parameter number. S value must be nearly 1.0 in a perfect situation.

4.4.3 Final Difference Map

The final difference map provides a real-space counterpart for checking how well the refined the model fits the experimental data, thus complimenting the R-factor which is a reciprocal-space measure. The final difference map should be featureless,

with no peaks or holes of a magnitude greater than a few estimated standard deviations of the map values.

4.4.4 Estimated Standard Deviations

Also we search for sensitivity of atomic parameters at the end of determination. In order to determine the structure sensitively, the standard deviations must be less than 0.001 for coordinates, 0.01Å for bond distances and 1° for angles.

CHAPTER FIVE

EXPERIMENTAL DETAILS
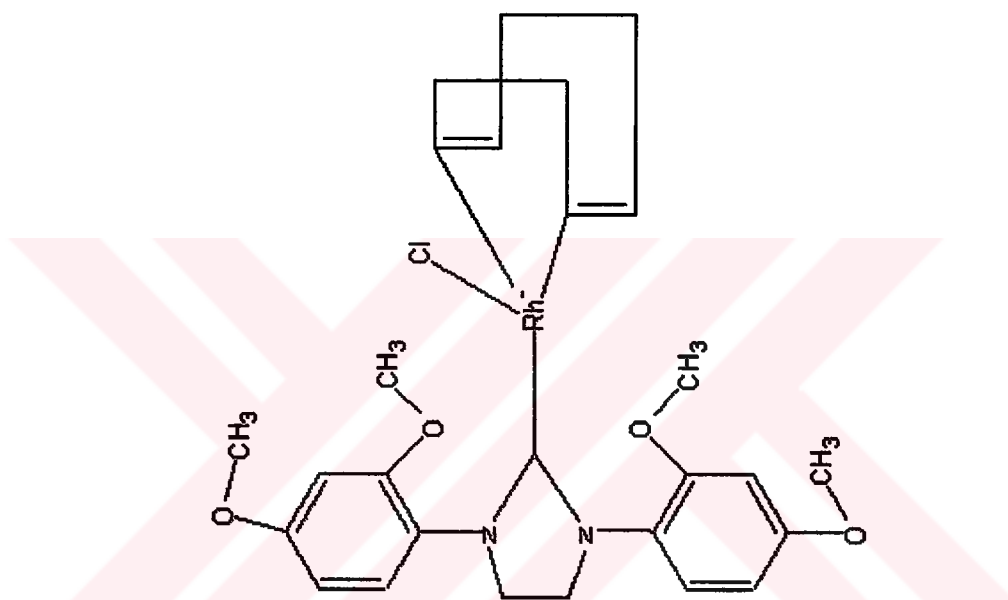
Figure 5.1 The chemical diagram of $C_{27}H_{34}N_2O_4ClRh$

5.1 Preparation of $C_{27}H_{34}N_2O_4ClRh$

A 50 ml Schlenk tube was charged with **(3)** (Figure 1.3) (0.240g., 0.52 mmol), $\left[RhCl(1,5-COD)\right]_2$ (0.124 g., 0.25 mmol) and 5 ml toluene. The solution was heated and then refluxed for 4 h. The resulting solution was cooled to room temperature and added hexane (10ml). The solid formed was filtered off and recrystallized from CH_2Cl_2/Et_2O .Yield: 0.193g. (66%), m.p.: 232-234 °C.

Anal. Cal. for $C_{27}H_{34}N_2O_4ClRh$; C: 55.01, H: 5.77, N: 4.75; found C: 54.87, H: 5.73, N: 4.56.

Results of spectroscopic investigation:

^1H -NMR ($\delta, CDCl_3$): 2.87 [s, 2H, COD-CH]; 4.52 [s, 2H, COD-CH]; 3.64 [t, 4H, J= 8.90 Hz, NCH_2CH_2N] and 4.25 [t, 4H, J= 8.91 Hz, NCH_2CH_2N]; 3.79 [s,12H, 2,4-^{13}C]; 6.46 [d, 2H, J= 2.47 Hz, 2,4-$(OCH_3)_2 C_6H_3$]; 6.58 [d, 2H, J=3.74 Hz, 2, 4-$(OCH_3)_2 C_6H_3$]; 8.29 [d, 2H, J= 8.68 Hz, 2, 4-$(OCH_3)_2 C_6H_3$].

^{13}C -NMR ($\delta, CDCl_3$): 28.7, 32.7 and 123.7 [COD- CH_2]; 97.6 [COD-CH]; 51.5 [NCH_2CH_2N]; [2,4-$(OCH_3)_2 C_6H_3$]; 55.8 [2,4-$(OCH_3)_2 C_6H_3$]; 56.0 [2,4-$(OCH_3)_2 C_6H_3$]; 99.1 [2,4-$(OCH_3)_2 C_6H_3$]; 104.0 [2,4-$(OCH_3)_2 C_6H_3$]; 132.9 [2,4-$(OCH_3)_2 C_6H_3$];155.9 [2,4-$(OCH_3)_2 C_6H_3$]; 160.3 [2,4-$(OCH_3)_2 C_6H_3$] (Günay et al., In press).

5.2 Data Collection of the Crystal

Before starting data collection, the suitable crystals were selected from the synthesized crystals by using stereomicroscope and polarization microscope. Than a sample of size $0.18 \times 0.30 \times 0.35$ mm^3 was selected for the crystallographic study.

The diffraction measurements were performed at room temperature $(293K)$ on an Enraf-Nonius CAD-4 diffractometer using graphite-monochromated MoK_α radiation. Orientation matrix and unit cell parameters were obtained from the setting angles of 25 reflections at medium θ ($3.0° < \theta < 44.3°$). The systematic absences and intensity symmetries indicated the triclinic P-1 space group. A total of 4650 intensities with θ_{max} = 44.3° were collected in the $w/2\theta$ scan mode, as suggested by peak-shape analyses. The crystal and equipment stabilities were checked by the intensities of three standard reflections monitored every 120 minutes. No considerable amount intensity decay was observed throughout measurement under

discussion. The intensities were corrected for Lorentz and Polarization factors and also for absorption effect $(\mu =0.809\,mm^{-1})$.

5.3 Structure Solution and Refinement of the Crystal

The structure was solved by Patterson methods using *SHELXS-86* for 2983 reflections with $I > 2\sigma\,(\,I\,)$. The position of the rhodium atom was determined from a three-dimensional Patterson map. The refinement (on F^2) was carried out by full-matrix least-squares procedure using *SHELXL-97*. All atoms were refined anisotropically, except for hydrogens. The structure was refined to $R = 0.041$ for the observed reflections and $R = 0.091$ for all data. The maximum and minimum peaks, observed in the final $\Delta\rho$ map, were 0.576 and –0.537 eA^{-3}, respectively. The scattering factors were taken from *SHELXL* – 97. All of the H atoms were add with HFIX. And positions and isotropic thermal parameters were refined. Further details of single crystal data measurement and refinement are given in Table 5.1. The atomic coordinates and equivalent isotropic thermal parameters of all atoms are listed in Table 5.2. Bond distances and angles are given Table 5.4 and Table 5.5. Anisotropic displacement parameters for $C_{27}H_{34}N_2O_4ClRh$ and torsion angles are listed in Table 5.3 and Table 5.6, respectively.

5.4 Experimental Results

Table 5.1 Crystallographic data for $C_{27}H_{34}N_2O_4ClRh$.

Crystal Data	
Chemical formula	$C_{27}H_{34}N_2O_4ClRh$
Color/shape	Yellow/prismatic
Formula weight	588.9
Space group	P-1 (No.2)
Crystal system	Triclinic
a, b, c (Å)	9.7642(12), 11.1914(11), 13.0102(14)

Crystal Data	
α, β, γ (°)	104.034(9), 106.658(9), 99.658(9)
Cell volume (Å^3)	1277.59(71)
Formula unit cell (Z)	2
D_x (g/cm^3)	1.531
F_{000}	607.9
Absorption coefficient μ(mm^{-1})	0.809
Crystal size (mm^3)	0.18 × 0.30 × 0.35

Data Collection	
Diffractometer	Enraf-Nonius CAD-4
Temperature (K)	293(2)
Scan type	W / 2θ
Radiation/Wavelength λ (Å)	MoK$_\alpha$ / 0.71073
Reflections measured	4650
Independent/observed reflections	4301/2983
Range of h,k,l	-11 → 0, -13 → 13, -16 → 16
Standard reflections	3
Standards interval time (min)	120
Absorption correction	ψ scan (North et al., 1968) T_{min} = 0.854, T_{max} = 0.980
Standard decay %	< % 2

Refinement	
Data/Restraints/Parameters	4301 / 0 / 316
Final R indices [I > 2σ (I)]	R_1 = 0.041, wR$_2$ = 0.091
R indices (all data)	R_1 = 0.091, wR$_2$ = 0.105

Weighting function	$w = \left[\sigma^2 (F_{obs}^2) + (0.0515P)^2 + 0.1106P \right]^{-1}$ $P = \frac{1}{3} \left(F_{obs}^2 + 2F_{cal}^2 \right)$
GOF $\left(on F^2 \right)$	1.025
$\Delta\rho_{min} / \Delta\rho_{max}$ (e/Å^3)	-0.537 / 0.576
$(\Delta / \sigma)_{max}$	0.087

Table 5.2 Atomic Coordinates and Equivalent Isotropic Thermal Parameters (Å^2)

Atom	x	y	z	U_{eq}^a
Rh1	0.4497(4)	0.3251(3)	0.1762(3)	0.0299(1)
Cl1	0.3948(1)	0.5152(1)	0.2658(1)	0.0492(5)
O1	0.0219(4)	0.0027(3)	0.3674(3)	0.0574(1)
O2	0.5066(3)	0.0226(3)	0.3528(3)	0.0502(1)
O3	0.9235(3)	0.3117(3)	0.2583(3)	0.0422(1)
O4	1.0400(4)	0.7188(3)	0.1926(4)	0.0549(1)
N1	0.5703(4)	0.2798(4)	0.4008(3)	0.0337(1)
N2	0.7390(4)	0.3946(4)	0.3630(3)	0.0318(1)
C1	-0.0882(6)	0.0655(6)	0.3888(6)	0.067(3)
C2	0.1556(5)	0.0783(5)	0.3809(4)	0.0411(2)
C3	0.1898(5)	0.2083(5)	0.4108(4)	0.0416(2)
C4	0.3276(5)	0.2737(5)	0.4164(4)	0.0405(2)
C5	0.4293(4)	0.2104(4)	0.3941(4)	0.0315(2)
C6	0.3963(5)	0.0785(4)	0.3679(4)	0.0372(2)
C7	0.2584(5)	0.0118(5)	0.3599(4)	0.0405(2)
C8	0.4827(5)	-0.1106(5)	0.3332(5)	0.0506(2)
C9	0.5942(4)	0.3331(4)	0.3252(4)	0.0291(1)
C10	0.7034(4)	0.2992(5)	0.4990(4)	0.0376(2)
C11	0.8169(5)	0.3917(5)	0.4768(4)	0.0379(2)
C12	0.8088(4)	0.4731(4)	0.3123(4)	0.0306(2)
C13	0.7898(5)	0.5934(5)	0.3203(4)	0.0403(2)

C14	0.8671(5)	0.6733(5)	0.2779(5)	0.0461(2)
C15	0.9654(5)	0.6319(5)	0.2283(4)	0.0397(2)
C16	0.9864(5)	0.5114(4)	0.2197(4)	0.0390(2)
C17	0.9077(4)	0.4308(4)	0.2606(4)	0.0297(2)
C18	0.9941(6)	0.2560(5)	0.1827(5)	0.0503(2)
C19	1.1187(6)	0.6760(5)	0.1219(5)	0.054(2)
C20	0.4320(5)	0.1306(5)	0.1051(5)	0.0444(2)
C21	0.5534(6)	0.2031(5)	0.0927(5)	0.0482(2)
C22	0.5622(7)	0.2357(7)	- 0.0119(5)	0.074(3)
C23	0.4377(7)	0.2815(6)	- 0.0712(5)	0.064(3)
C24	0.3637(6)	0.3468(5)	0.0065(4)	0.0438(2)
C25	0.2481(5)	0.2826(5)	0.0285(4)	0.0421(2)
C26	0.1822(5)	0.1421(5)	-0.0150(5)	0.063(2)
C27	0.2861(6)	0.0622(5)	0.0106(6)	0.075(2)
H1A	-0.17630	0.00300	0.37680	0.1000
H1B	-0.11040	0.11530	0.33860	0.1000
H1C	-0.05160	0.12020	0.46540	0.1000
H3	0.12200	0.25240	0.42700	0.0500
H4	0.35100	0.36210	0.43570	0.0480
H7	0.23460	-0.07660	0.34070	0.0480
H8A	0.56850	-0.13630	0.32390	0.0770
H8B	0.39850	-0.15430	0.26620	0.0770
H8C	0.46480	-0.13160	0.39640	0.0770
H10A	0.73130	0.22020	0.49980	0.0450
H10B	0.68920	0.33650	0.56950	0.0450
H11A	0.84510	0.47550	0.53150	0.0460
H11B	0.90470	0.36110	0.47920	0.0460
H13	0.72450	0.62160	0.35440	0.0490
H14	0.85290	0.75440	0.28290	0.0560
H16	1.05310	0.48430	0.18650	0.0460
H18A	0.99980	0.17270	0.18780	0.0750
H18B	1.09200	0.30870	0.20300	0.0750

H18C	0.93760	0.24930	0.10690	0.0750
H19A	1.16650	0.74660	0.10420	0.0820
H19B	1.05140	0.61330	0.05350	0.0820
H19C	1.19170	0.63880	0.15970	0.0820
H20	0.45880	0.08600	0.16110	0.0530
H21	0.64850	0.19950	0.14210	0.0580
H22A	0.65320	0.30080	0.00910	0.0890
H22B	0.56850	0.16060	-0.06450	0.0890
H23A	0.36460	0.20970	-0.13030	0.0770
H23B	0.47400	0.34080	-0.10650	0.0770
H24	0.36140	0.43400	0.00650	0.0530
H25	0.17810	0.33260	0.04180	0.0500
H26A	0.10490	0.12260	0.01600	0.0750
H26B	0.13570	0.11820	-0.09620	0.0750
H27A	0.30670	0.02570	-0.05730	0.0910
H27B	0.23760	-0.00770	0.03000	0.0910

U_{eq}^{a} is defined as one third of the trace of the orthogonalized U_{ij} tensor.

The Uiso values for C atoms range from 0.0291(1) $Å^2$ to 0.075(2) $Å^2$, while Uiso values for H atoms are in the range 0.0450-0.1000 $Å^2$.

Table 5.3 Anisotropic displacement parameters ($Å^2$)

Atom	U_{11}	U_{22}	U_{33}	U_{23}	U_{13}	U_{12}
Rh1	0.022(2)	0.036(2)	0.028(2)	0.006(2)	0.006(1)	0.006(1)
Cl1	0.044(7)	0.047(8)	0.051(9)	0.004(7)	0.016(6)	0.018(5)
O1	0.034(2)	0.053(2)	0.086(3)	0.021(2)	0.030(2)	-0.0005(2)
O2	0.040(2)	0.041(2)	0.076(3)	0.019(2)	0.028(2)	0.008(2)
O3	0.044(2)	0.044(2)	0.050(3)	0.024(2)	0.024(2)	0.014(2)
O4	0.057(2)	0.048(2)	0.063(3)	0.026(2)	0.026(2)	-0.0008(2)

N1	0.026(2)	0.045(2)	0.029(3)	0.018(2)	0.006(2)	0.0007(2)
N2	0.022(2)	0.047(2)	0.026(2)	0.014(2)	0.008(2)	0.002(2)
C1	0.039(3)	0.076(4)	0.100(6)	0.037(4)	0.040(3)	0.010(3)
C2	0.031(2)	0.048(3)	0.044(3)	0.015(3)	0.017(2)	0.001(2)
C3	0.032(2)	0.053(3)	0.045(4)	0.018(3)	0.017(2)	0.013(2)
C4	0.033(2)	0.040(3)	0.046(3)	0.015(2)	0.012(2)	0.003(2)
C5	0.026(2)	0.042(3)	0.025(3)	0.014(2)	0.009(2)	-0.0009(2)
C6	0.029(2)	0.044(3)	0.037(3)	0.010(2)	0.014(2)	0.004(2)
C7	0.036(3)	0.036(3)	0.047(4)	0.013(2)	0.016(2)	0.001(2)
C8	0.045(3)	0.044(3)	0.056(4)	0.007(3)	0.018(3)	0.005(2)
C9	0.020(2)	0.033(2)	0.027(3)	0.002(2)	0.004(2)	0.004(2)
C10	0.028(2)	0.055(3)	0.029(3)	0.017(2)	0.006(2)	0.009(2)
C11	0.027(2)	0.051(3)	0.031(3)	0.017(2)	0.004(2)	0.001(2)
C12	0.024(2)	0.042(3)	0.021(3)	0.014(2)	0.002(2)	-0.0007(2)
C13	0.034(2)	0.048(3)	0.041(4)	0.016(3)	0.015(2)	0.009(2)
C14	0.043(3)	0.039(3)	0.056(4)	0.018(3)	0.014(2)	0.010(2)
C15	0.033(2)	0.044(3)	0.036(3)	0.016(2)	0.006(2)	-0.001(2)
C16	0.032(2)	0.041(3)	0.043(3)	0.013(2)	0.012(2)	0.008(2)
C17	0.025(2)	0.036(3)	0.026(3)	0.013(2)	0.004(2)	0.004(2)
C18	0.057(3)	0.048(3)	0.048(4)	0.011(3)	0.021(3)	0.019(3)
C19	0.057(3)	0.061(4)	0.045(4)	0.026(3)	0.019(3)	-0.002(3)
C20	0.050(3)	0.033(3)	0.040(3)	0.008(2)	0.001(2)	0.014(2)
C21	0.046(3)	0.062(4)	0.037(3)	0.007(3)	0.012(2)	0.031(3)
C22	0.068(4)	0.127(6)	0.046(4)	0.029(4)	0.029(3)	0.053(4)
C23	0.078(4)	0.086(5)	0.048(4)	0.030(3)	0.034(3)	0.034(3)
C24	0.054(3)	0.052(3)	0.033(4)	0.021(3)	0.013(2)	0.025(3)
C25	0.033(2)	0.057(3)	0.031(3)	0.013(3)	0.000(2)	0.018(2)
C26	0.035(3)	0.063(4)	0.061(4)	-0.003(3)	-0.006(2)	0.009(2)
C27	0.050(3)	0.043(3)	0.095(6)	0.002(3)	-0.009(3)	0.001(3)

Looking at the values of anisotropic displacement parameters in table, abnormal values have not been appeared.
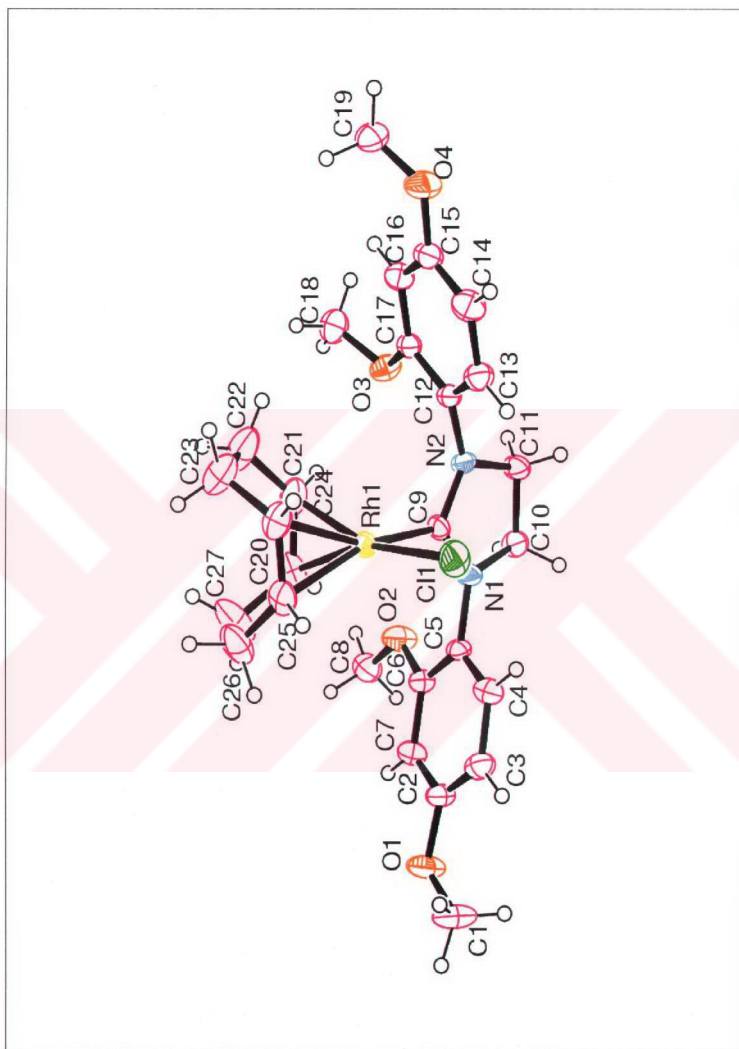
Figure 5.2 An ORTEP3 drawing of the title compound showing the atomic numbering scheme. Displacement ellipsoids of non-H atoms are shown at % 40 probability level; H atoms are shown as small spheres of arbitrary size.

Table 5.4 Bond distances (Å)

Atoms	Bond Distance	Atoms	Bond Distance
Rh1-Cl1	2.390(2)	C12-C17	1.407(6)
Rh1-C9	2.015(5)	C13-C14	1.387(8)
Rh1-C20	2.105(6)	C14-C15	1.383(7)
Rh1-C21	2.109(6)	C15-C16	1.381(7)
Rh1-C24	2.215(5)	C16-C17	1.386(7)
Rh1-C25	2.207(5)	C20-C21	1.393(8)
O1-C1	1.434(8)	C20-C27	1.517(9)
O1-C2	1.370(7)	C21-C22	1.513(9)
O2-C6	1.370(6)	C22-C23	1.483(1)
O2-C8	1.416(7)	C23-C24	1.522(9)
O3-C17	1.361(6)	C24-C25	1.373(8)
O3-C18	1.438(7)	C25-C26	1.492(8)
O4-C15	1.367(7)	C26-C27	1.481(8)
O4-C19	1.408(8)	C1-H1A	0.9601
N1-C5	1.430(6)	C1-H1B	0.9592
N1-C9	1.322(6)	C1-H1C	0.9603
N1-C10	1.479(6)	C3-H3	0.9303
N2-C9	1.351(6)	C4-H4	0.9299
N2-C11	1.469(6)	C7-H7	0.9300
N2-C12	1.417(6)	C8-H8A	0.9598
C2-C3	1.367(8)	C8-H8B	0.9604
C2-C7	1.395(7)	C8-H8C	0.9614
C3-C4	1.392(8)	C10-H10A	0.9694
C4-C5	1.369(7)	C10-H10B	0.9703
C5-C6	1.390(7)	C11-H11A	0.9691
C6-C7	1.388(7)	C11-H11B	0.9703
C10-C11	1.525(7)	C13-H13	0.9299
C12-C13	1.373(7)	C14-H14	0.9306

C16-H16	0.9310	C22-H22B	0.9701
C18-H18A	0.9601	C23-H23A	0.9693
C18-H18B	0.9602	C23-H23B	0.9691
C18-H18C	0.9596	C24-H24	0.9799
C19-H19A	0.9598	C25-H25	0.9795
C19-H19B	0.9609	C26-H26A	0.9705
C19-H19C	0.9598	C26-H26B	0.9700
C20-H20	0.9795	C27-H27A	0.9706
C21-H21	0.9797	C27-H27B	0.9695
C22-H22A	0.9706		

The C-H bond distances range from 0.9299 Å to 0.9799 Å.

Table 5.5 Bond Angles (°)

Atoms	Bond Angles	Atoms	Bond Angles
Cl1-Rh1-C9	90.03(1)	C2-C3-C4	119.0(5)
Cl1-Rh1-C20	160.6(2)	C3-C4-C5	121.3(5)
Cl1-Rh1-C21	160.8(2)	N1-C5-C4	120.2(4)
Cl1-Rh1-C24	93.0(2)	N1-C5-C6	120.2(4)
Cl1-Rh1-C25	90.5(2)	C4-C5-C6	119.6(4)
C9-Rh1-C20	92.7(2)	O2-C6-C5	116.2(4)
C9-Rh1-C21	89.3(2)	O2-C6-C7	124.0(4)
C9-Rh1-C24	160.0(2)	C5-C6-C7	119.8(5)
C9-Rh1-C25	163.6(2)	C2-C7-C6	119.5(5)
C20-Rh1-C21	38.6(2)	Rh1-C9-N1	128.5(3)
C20-Rh1-C24	91.0(2)	Rh1-C9-N2	123.6(3)
C20-Rh1-C25	81.5(2)	N1-C9-N2	107.8(4)
C21-Rh1-C24	81.4(2)	N1-C10-C11	100.9(4)
C21-Rh1-C25	95.4(2)	N2-C11-C10	103.6(4)

C24-Rh1-C25	36.2(2)	N2-C12-C13	120.9(4)
C1-O1-C2	117.2(4)	N2-C12-C17	119.4(4)
C6-O2-C8	118.7(4)	C13-C12-C17	119.5(4)
C17-O3-C18	116.2(4)	C12-C13-C14	120.6(5)
C15-O4-C19	118.3(4)	C13-C14-C15	119.7(5)
C5-N1-C9	125.0(4)	O4-C15-C14	115.4(5)
C5-N1-C10	120.3(4)	O4-C15-C16	124.0(5)
C9-N1-C10	114.6(4)	C14 -C15-C16	120.6(5)
C9-N2-C11	112.2(4)	C15-C16-C17	119.8(5)
C9-N2-C12	126.3(4)	O3-C17-C12	116.2(4)
C11-N2-C12	120.6(4)	O3-C17-C16	124.0(4)
O1-C2-C3	124.7(5)	C12-C17-C16	119.8(4)
O1-C2 -C7	114.5(5)	Rh1-C20-C21	70.8(3)
C3-C2-C7	120.8(5)	Rh1-C20-C27	113.0(4)
C21-C20-C27	124.7(5)	O2-C8-H8C	109.45
Rh1-C21-C20	70.6(3)	H8A-C8-H8B	109.51
Rh1-C21-C22	110.0(4)	H8A-C8-H8C	109.42
C20-C21-C22	127.5(6)	H8B-C8-H8C	109.42
C21-C22-C23	115.9(6)	N1-C10-H10A	111.61
C22-C23-C24	113.2(5)	N1-C10-H10B	111.58
Rh1-C24-C23	110.8(4)	C11-C10-H10A	111.61
Rh1-C24-C25	71.6(3)	C11-C10-H10B	111.56
C23-C24-C25	123.2(5)	H10A-C10-H10B	109.41
Rh1-C25-C24	72.2(3)	N2-C11-H11A	111.05
Rh1-C25-C26	108.8(4)	N2-C11-H11B	110.98
C24-C25-C26	125.8(5)	C10-C11-H11A	111.09
C25-C26-C27	115.9(5)	C10-C11-H11B	111.01
C20-C27-C26	115.4(5)	H11A-C11-H11B	109.08
O1-C1-H1A	109.49	C12-C13-H13	119.72
O1-C1-H1B	109.47	C14-C13-H13	119.68
O1-C1-H1C	109.47	C13-C14-H14	120.14
H1A-C1-H1B	109.46	C15-C14-H14	120.17

H1A-C1-H1C	109.45	C15-C16-H16	120.14
H1B-C1-H1C	109.48	C17-C16-H16	120.09
C2-C3-H3	120.52	O3-C18-H18A	109.38
C4-C3-H3	120.52	O3-C18-H18B	109.52
C3-C4-H4	119.35	O3-C18-H18C	109.47
C5-C4-H4	119.37	H18A-C18-H18B	109.47
C2-C7-H7	120.17	H18A -C18-H18C	109.48
C6-C7-H7	120.31	H18B-C18-H18C	109.50
O2-C8-H8A	109.51	O4-C19-H19A	109.50
O2-C8-H8B	109.52	O4-C19-H19B	109.44

Table 5.6 Torsion Angles (°)

Atoms	Torsion Angles	Atoms	Torsion Angles
Cl1-Rh1-C9-N1	91.8(4)	Cl1-Rh1-C9-N2	-90.2(4)
C20-Rh1-C9-N1	-69.0(5)	C20-Rh1-C9-N2	109.1(4)
C21-Rh1-C9-N1	-107.4(5)	C21-Rh1-C9-N2	70.6(4)
C9-Rh1-C20-C21	-85.5(4)	C9-Rh1-C20-C27	154.1(4)
C21-Rh1-C20-C27	-120.4(6)	C24-Rh1-C20-C21	74.8(4)
C24-Rh1-C20-C27	-45.6(4)	C25-Rh1-C20-C21	109.9(4)
C25-Rh1-C20-C27	-10.6(4)	C9-Rh1-C21-C20	95.2(4)
C9-Rh1-C21-C22	-140.9(4)	C20-Rh1-C21-C22	123.9(6)
C24-Rh1-C21-C20	-102.6(4)	C24-Rh1-C21-C22	21.3(4)
C25-Rh1-C21-C20	-69.1(4)	C25-Rh1-C21-C22	54.8(4)
Cl1-Rh1-C24-C23	153.8(4)	Cl1-Rh1-C24-C25	-86.9(3)
C20-Rh1-C24-C23	-45.2(4)	C20-Rh1-C24-C25	74.1(3)
C21-Rh1-C24-C23	-7.7(4)	C21-Rh1-C24-C25	111.6(4)
C25-Rh1-C24-C23	-119.4(6)	Cl1-Rh1-C25-C24	94.3(3)
Cl1-Rh1-C25-C26	-143.0(3)	C20-Rh1-C25-C24	-103.5(4)
C20-Rh1-C25-C26	19.2(4)	C21-Rh1-C25-C24	-67.4(4)
C21-Rh1-C25-C26	55.3(4)	C24-Rh1-C25-C26	122.7(5)

C1-O1-C2-C3	-1.5(7)	C1-O1-C2-C7	179.4(5)
C8-O2-C6-C7	-3.2(7)	C8-O2-C6-C5	175.9(4)
C18-O3-C17-C12	165.1(4)	C18-O3-C17-C16	-17.4(7)
C19-O4-C15-C14	-167.5(5)	C19-O4-C15-C16	14.2(8)
C9-N1-C10-C11	6.6(5)	C5-N1-C9-N2	177.2(4)
C10-N1-C9-N2	-1.4(6)	C5-N1-C9-Rh1	-4.5(7)
C9-N1-C5-C4	-75.2(6)	C10-N1-C5-C4	103.4(6)
C10-N1-C9-Rh1	176.9(3)	C5-N1-C10-C11	-172.1(4)
C9-N1-C5-C6	106.6(6)	C10-N1-C5-C6	-74.9(6)
C11-N2-C12-C13	-93.9(6)	C9-N2-C12-C13	74.6(6)
C11-N2-C12-C17	81.2(6)	C11-N2-C9-Rh1	176.6(3)

Table 5.7 Hydrogen bonds (Å).

D	H	A	D—H	H...A	D...A	D—H...A (°)
C10	-- H10B	.. Cl1	0.9703	2.7846	3.723(5)	162.88
C21	-- H21	.. O3	0.9797	2.5871	3.460(7)	148.40

Symmetry operation: ($1-x, 1-y, 1-z$)

The crystal structure has two intermolecular hydrogen bonds of the type C-H....Cl and C-H....O.

Table 5.8 Standard deviations of atoms from the some remarkable planes $(°)$.

Plane 1		Plane 2		Plane 3		Plane 4	
Atoms	Deviations (Å)	Atoms	Deviations (Å)	Atoms	Deviations (Å)	Atoms	Deviations (Å)
* Rh1	0.015(1)	* N1	0.027(4)	* C2	-0.012(5)	* C12	0.003(5)
* Cl1	-0.007(1)	* N2	-0.044(4)	* C3	0.012(5)	* C13	0.003(5)
* C20	-0.004(6)	* C9	0.010(5)	* C4	0.001(5)	* C14	-0.005(6)
* C21	-0.004(6)	* C10	-0.048(5)	* C5	-0.014(5)	* C15	-0.001(5)
O4	0.643(4)	* C11	0.054(5)	* C6	-0.014(5)	* C16	-0.004(5)
C1	1.400(7)	Rh1	0.006(1)	* C7	-0.001(5)	* C17	-0.006(5)
C14	1.114(6)	O1	0.363(4)	O1	-0.065(4)	O2	-1.048(3)
		O4	0.390(4)	O2	0.072(4)	N1	-0.324(4)
		C23	-1.485(7)	N1	-0.020(4)	C5	-1.013(5)
				C12	-1.451(5)	C10	1.104(5)

* The atoms that constituted the planes.

The equation of planes:

Plane 1: $3.44(5)\,x - 4.00(4)\,y + 10.35(2)\,z = 2.06(2)$

Plane 2: $-5.34(2)\,x + 8.78(2)\,y + 4.74(3)\,z = 1.28(2)$

Plane 3: $0.76(2)\,x - 2.80(2)\,y + 12.10(1)\,z = 4.52(3)$

Plane 4: $4.41(2)\,x + 0.14(2)\,y + 8.50(2)\,z = 6.28(1)$

Table 5.9 Dihedral angles between the planes $(°)$.

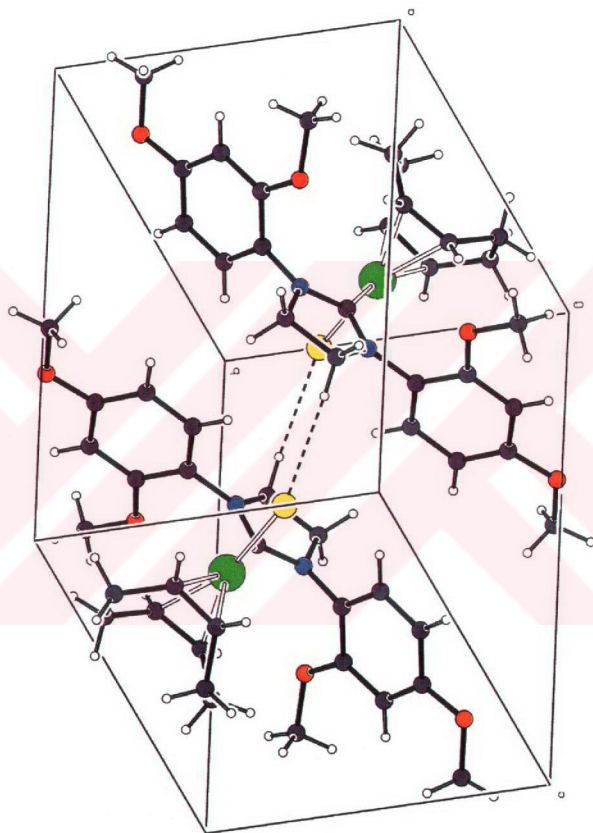| Planes	Dihedral angle
1-2	89.8(4)
1-3	80.5(4)
2-3	76.8(3)
2-4	77.3(3)
3-4	29.3(2)

Figure 5.3 The dimeric structure occurred by intermolecular hydrogen bonds in the unit cell.
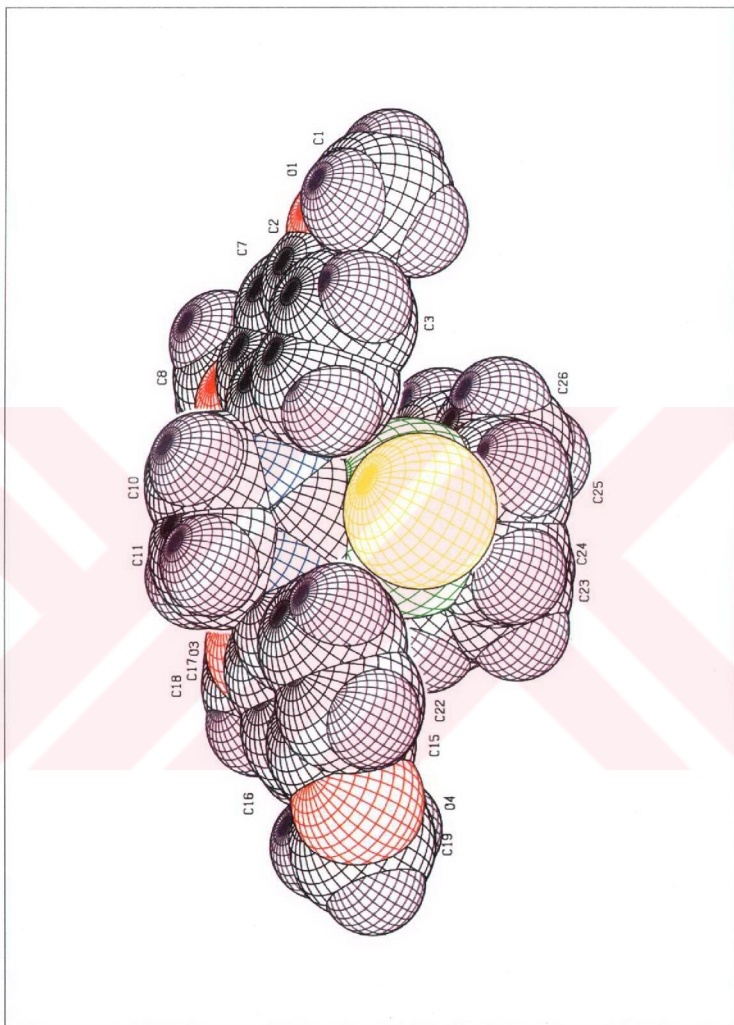
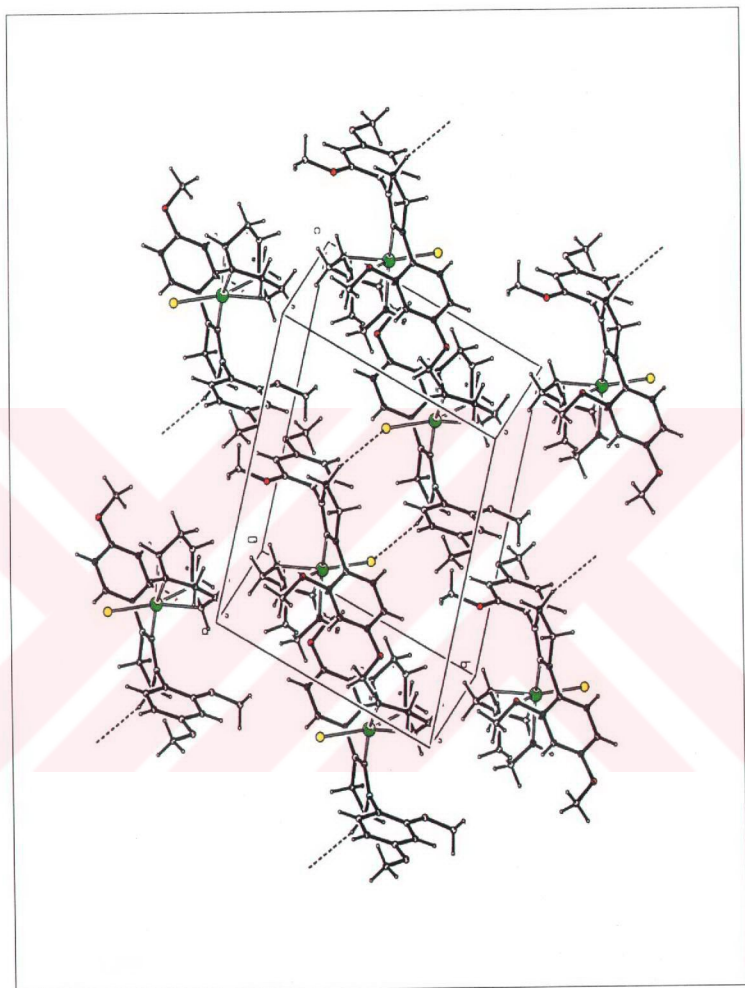**Figure 5.4** A CPK drawing of $C_{27}H_{34}N_2O_4ClRh$.

Figure 5.5 Unit cell packing diagram of $C_{27}H_{34}N_2O_4ClRh$.

CHAPTER SIX
CONCLUSION

In this study, molecular and crystal structures of 1,3-Bis(2,4-dimethoxyphenyl)imidazolidin-2-ylidenechloro(1,5-cyclooctadiene)rhodium(I), $C_{27}H_{34}N_2O_4ClRh$, has been determined by single crystal X-ray diffraction technique and then following results have been concluded.

Complexes of heterocyclic carbenes are thought to involve only a single M-C bond. Experimental X-ray evidence shows M-C(carbene) bond lengths are virtually the same as M-C(hydrocarbyl) single bonds (Herrmann (b) et al., 1995) and ab initio studies show π-back bonding is not significant with these ligands (Fröhlich et al., 1997).The donation of electron density by the nitrogen substituents on the carbene makes the carbene carbon nucleophilic and compensates for the electron flow from the carbon to the metal. Donation from the nitrogens is such that the carbene carbon may actually become a partial π-donor (Herrman (b) et al., 1995; Fröhlich et al., 1997). Heterocyclic carbenes are thus pure donor ligands (Lappert, 1975).

In our study, the distances between the rhodium and the carbene carbon d(Rh-C9) = 2.015(5)Å and between the rhodium and the chloro atom d(Rh-Cl) = 2.3900(15)Å are in the expected range. For the same type studies, the bond distances take value d(Rh-$C_{carbene}$) = 2.029(4)Å, d(Rh-Cl) = 2.372(1)Å (Danopoulos et al.,2002); d(Rh-$C_{carbene}$) = 2.021(3)Å (Herrmann (b) et al.,1997); d(Pd-$C_{carbene}$) = 2.009(8)Å, d(Pd-Cl) = 2.3996(9)Å (McGuinness et al., 1998).

As shown in Table 5.4 the Rh-C_{cod} bond lengths are d(Rh-C20) = 2.105(6)Å, d(Rh-C21) = 2.109(6)Å, d(Rh-C24) = 2.215(5)Å, d(Rh-C25) = 2.207(5)Å. The bond lengths of the Rh-C20 and Rh-C21 are shorter than the Rh-C24 and Rh-C25. The reason of this attributed to trans influences of the chelating ligand in Figure 5.1. These results agree with the values of the literatures (Ingleson et al., 2001; Vicente et al., 2001).

The C(carbene)-N bond lengths in our complex d(N1-C9) = 1.322(6)Å and d(N2-C9) = 1.351(6)Å. This is significantly shorter than the other C-N bond lengths present in the complexes, for instance d(N1-C10) = 1.479(6)Å, and is possibly indicative of greater partial double bond character in these C(carbene)-N bonds due to partial electron donation by nitrogen to the carbene carbon. The theoretical studies also indicated that the stability of these carbenes is due to electron donation from the nitrogen lone pairs into the formally vacant p(π) orbital of the carbene carbon (McGuinness et al., 1998).

As it is published for analogous rhodium carbene complexes, the atoms Rh1, Cl1, C20, C21 form a plane. Also the carbene ligand is nearly planar. The angle of 89.8(4)°, between the carbene heterocycle and the coordination plane, is in agreement with the values of the literatures (Herrmann (b) et al., 1997; Herrmann (a) et al., 1996).

Cl-Rh-$C_{carbene}$ angle 90.0(1)° is in consistence with this type of compounds in the literatures (Danopoulos et al., 2002; Herrmann (b) et al., 1997). The imidazole heterocycle makes dihedral angles of 76.8(3)° and 77.3(3)° with the methoxyphenyl ring planes, respectively. In addition the dihedral angle between two methoxyphenyl ring planes is 29.3(2)°.

The molecule exhibits intermolecular hydrogen bonds of the type C-H...O and C-H...Cl. C21-H21...O3 has length 3.460(6) Å and C10-H10B...Cl1 has length 3.722(5) Å with symmetry code 1-x, 1-y, 1-z.The bond lengths are in good agreement with those of similar complexes (Lokanath et al., 2001; Bujak & Zaleski, 2002; Stanley et

al., 2003). And as shown in Figure 5.3 the crystal structure is stabilized by two weak intermolecular hydrogen bond between C(10)...Cl(1).

REFERENCES

Arduengo, A. J., Rasika Dias, H. V., Harlow, R. L. & Kline, M. (1992). J. Am. Chem. Soc., 114, 5530.

Aygün, M. (1997). Tek Kristal X-Işınları Kırınımı Yöntemiyle $C_{12}H_{14}O_4N_4S$ $C_{16}H_{18}ClO_2PS$ ve $C_{17}H_{15}ClO_3$ Moleküllerinin Kristal Yapı Çözümü. Samsun: Doktora Tezi.

Bourissou, D., Guerret, O., Gabbai, F. P. & Bertrand, G. (2000). Chem. Rev., 100, 39.

Bujak, M. & Zaleski, J. (2002). Crystal and Molecular Structure of Bis (N, N-Dimethylethylenediammonium) Hexadecachlorotetraantimonate(III) $\left[\left(CH_3 \right)_2 NH \left(CH_2 \right)_2 NH_3 \right]_2 \left[Sb_4Cl_{16} \right]$ at 295 and 95 K. A structurally Novel $\left[Sb_4Cl_{16} \right]^{4-}$ Anion. Main Group Metal Chemistry, 25, 571-577.

Çetinkaya, B., Özdemir, I. & Dixneuf, P. H. (1997). Synthesis and catalytic properties of N-functionalized carbene complexes of rhodium(I) and ruthenium(II). Journal of Organometallic Chemistry, 534, 153-158.

Danopoulos, A. A., Winston S. & Hursthouse, M. B. (2002). C-H activation with N-heterocyclic carbene complexes of Iridium and Rhodium. J. Chem. Soc. Dalton Trans., 3090-3091.

Dunbar, K. R. & Quillevere, A. (1993). An Unusual Heterobimetallic Compound

with a Rhodium(I)-η^4-Arene Interaction. Organometallics, 12, 618-620.

Farrugia, L. J. (1997). Ortep3 for Windows. Journal of Aplied Crystallography, 30, 565.

Farrugia, L. J. (1999). WinGX. Journal of Applied Crystallography, 32, 837-838.

Fröhlich, N., Pidun, U., Stahl, M. & Frenking, G. (1997). Organometallics, 16, 442.

Giacovazzo, C., Monaco, H. L., Viterbo, D., Scordari, F., Gilli, G., Zanotti, G. & Catti, M. (1998). Fundamentals of Crystallography. Oxford: Oxford University Press.

Glusker, J. P. & Trueblood, K. N. (1972). Crystal Structure Analysis: A Primer. New York: Oxford University Press.

Green, M. J., Cavell, K. J., Skelton, B. W. & White, A. H. (1998). A route to new methylpalladium(II) carbene complexes. Journal of Organometallic Chemistry, 554, 175-179.

Günay, M. E., Aygün, M., Çetinkaya, B. & Kartal, A. (In press).

(a)Herrmann, W. A., Elison, M., Fischer, J., Köcher, C. & Artus, G. R. J. (1995). Angew. Chem., 121, 2602-2605.

(b) Herrmann, W. A., Elison, M., Fischer, J., Köcher, C. & Artus, G. R. J. (1995). Angew. Chem. Int. Edn. Engl., 34, 2371-2374.

(a) Herrmann, W. A., Elison, M., Fischer, J., Köcher, C. & Artus, G. R. J. (1996). Chem. Eur. J., 2, 772.

(b) Herrmann, W. A., Gooben, L. J., Köcher, C. & Artus, G. R. J. (1996). Angew.

Chem., 108, 2980-2982.

(c) Herrmann, W. A., Gooben, L. J., Köcher, C. & Artus, G. R. J. (1996). Angew. Chem. Int. Edn. Engl., 35, 2805-2807.

(a) Herrmann, W. A. & Köcher, C. (1997). Angew. Chem., Int. Ed. Engl., 36, 2163.

(b) Herrmann, W. A., Gooben, L. J. & Spiegler, M. (1997). Functionalized imidazoline-2- ylidene complexes of rhodium and palladium. Journal of Organometallic Chemistry, 547, 357-366.

Herrmann, W. A., Reisinger, C. P. & Spiegler, M. (1998). Chelating N-heterocyclic Carbene ligands in palladium-catalyzed heck-type reactions. Journal of Organometallic Chemistry, 557, 93-96.

Herrmann, W. A. (2002). Angew. Chem. Int. Ed., 41, 1291.

Huang, J., Schanz, H. J., Stevens, E. D. & Nolan, S. P. (1999). Organometallics, 18, 2370.

Ingleson, M., Patmore, N. J., Ruggiero, G. D., Frost, C. G., Mahon, M. F., Willis, M. C. & Weller A. S. (2001). Chelating Monoborane Phosphines: Rational and High-Yield Synthesis of

$$\left[(COD)Rh\{(\eta^2 - BH_3)Ph_2PCH_2PPh_2\}\right][PF_6](COD = 1,5 - cyclooctadiene).$$
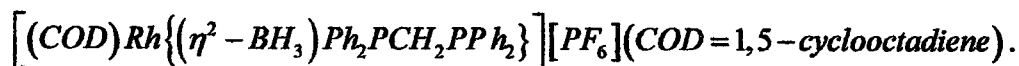
Organometallics, 20, 4434-4436.

Lappert, M. F. (1988). J. Organomet. Chem., 534, 153.

Lappert, M. F. (1975). J. Organomet. Chem., 100, 139.

Lecture Notes for the Tenth Summer School " Course In Crystallography". (2001).

Structure Analysis by X-Ray Crystallography. (4th ed.). American Crystallographic Association: University of Georgia.

Lokanath, N. K., Anandalwar, S. M., Prasad, J. S. & Ramappa, P. G. (2001). Crystal Structure of Diphenyl Pyraline Tetrachloroferrate. Analytical Sciences, 17, 1135-1136.

McGuinness, D. S., Green, M. J., Cavell, K. J., Skelton, B. W. & White, A. H. (1998). Synthesis and reaction chemistry of mixed ligand methylpalladium-carbene complexes. Journal of Organometallic Chemistry, 565, 165-178.

North, A. C. T., Phillips, D.C. & Mathews, F. S. (1968). Acta Cryst., A24, 351.

Sheldrick, G. M. (1990). Shelxs-86, University of Göttingen, Germany.

Sheldrick, G. M. (1998). Shelxl-97, University of Göttingen, Germany

Spek, A. L. (1990). Platon-Pluton. Acta Crysallographica, A46, C34.

Spannenberg, A., Fdil, N., Firdoussi, L. E. & Karim, A. (2002). Crystal structure of [(1R)-(+)-3-benzoly-camphoryl-O,O'](cycloocta-1,5-diene)rhodium(I), $C_{25}H_{31}O_2Rh$. Z. Kristallogr. NCS, 217, 549-550.

Stanley, N., Muthiah, P. T. & Geib, S. J. (2003). N^6-Furfuryladenine (kinetin) hydrochloride. Acta Crystallographica, C59, 27-29.

Stout, G. H. & Jensen, L. H. (1989). X-Ray Structure Determination. John Wiley & Sons: New York, Chichester, Brisbane, Toronto & Singapore.

Vazquez-Serrano, L. D., Owens, B. T. & Buriak, J. M.(2002). Catalytic olefin hydrogenation using N-heterocyclic carbene-phosphine complexes of iridium. Chem. Commun., 2518-2519.

Vicente, J., Gil-Rubio, J. & Bautista, D. (2001).Synthesis and Reactivity of Fluoro Complexes. Part 1. Cyclooctadiene Rhodium(I) Complexes. Inorganic Chemistry, 40, 2636-2637.

Weskamp, T., Kohl, F. J. & Herrmann, W. A. (1999). N-heterocyclic carbenes: novel ruthenium-alkylidene complexes. Journal of Organometallic Chemistry, 582, 362- 365.

Weskamp, T., Böhm, V. P. W. & Herrmann, W. A. (2000). J. Organomet. Chem., 600, 12.

Yang, F. & Hamilton, J. H. (1996). Modern Atomic and Nuclear Physics. New York: McGraw-Hill.

Yıldırım, Ö. (2002). Diaminocarbene Complexes Containing Ferrocene. İzmir: Yüksek Lisans Tezi.